Opto-Electronic Science

Review

2022, Vol. 1, No. 8

DOI: 10.29026/oes.2022.220003

Terahertz generation from laser-induced plasma

Wenfeng Sun[1,2], Xinke Wang[1,2] and Yan Zhang[1,2]*

Interest of the research in terahertz (THz) wave has been strongly motivated by its wide applications in the fields of physics, chemistry, biology, and engineering. Developing efficient and reliable THz source is of uttermost priority in these researches. Numerous attempts have been made in fulfilling the THz generation. Greatly benefited from the progress of the ultrafast pulses, the laser-induced-plasma is one of the auspicious tools to provide desirable THz waves, owing to its superiorities in high power threshold, intense THz signal, and ultrawide THz spectrum. This paper reviews the physics and progress of the THz generation from the laser-induced plasmas, which are produced by gas, liquid, and solid. The characteristics of the emitted THz waves are also included. There are many complicated physical processes involved in the interactions of laser-plasma, making various laser-plasma scenarios in the THz generations. In view of this, we will only focus on the THz generation classified by physical mechanisms. Finally, we discuss a perspective on the future of THz generation from the laser-induced plasma, as well as its involved challenges.

Keywords: terahertz generation; ultrafast pulses; laser-induced plasma

Sun WF, Wang XK, Zhang Y. Terahertz generation from laser-induced plasma. *Opto-Electron Sci* **1**, 220003 (2022).

Introduction

Terahertz (THz) band is sandwiched between the microwave (MW) and infrared (IR) in the electromagnetic spectrum, spanning from 0.1 THz to 10 THz. The THz waves can be accessed by electronics and photonics technologies. In the last decades, the continuous supplies of new devices and materials by the progresses in the fields of photonics and electronics have bridged the THz gap. As it is an area of convergence between the fields of electronics and photonics, there are many significant features in the THz band. Photo energy at 1 THz is only 4.3 meV, far lower than that of an X-ray photon. At such energy level, ionizing a living cell with a THz source seems to be hard. Therefore, unlike the X-ray, the THz radiation is relatively safe for the sample to be detected; Compared with IR, Mie scattering hardly happens to the THz waves, owning to its longer wavelength. Therefore, it is transparent for non-polar and non-conducting materials, such as plastic, paper, and cloth, which makes it promising in the nondestructive evaluation. As the dipole-allowed rotational and vibrational transition of molecules undergoing within the THz range, so it features signature fingerprint in the forms of the THz spectrum; As the wavelength of THz wave is on the order of tens micrometers, the spatial resolution is higher than that of MW when it is used in imaging. With these performances, it has been proved to be particularly valuable in the characterization of semiconductor[1–3], biology[4–6], diagnose the dynamics of water molecules[7], non-destructive testing[8–10], homeland security[9], and THz communication[11–13]. Instead of using weak fields to observed THz modes, one can also use strong THz field to actively trigger nonlinear THz responses of materials[14–25], induces the materials to a new state[26–31], rapid phase transitions[32] or even THz atom probe microscopy[33].

Impressive advance has been achieved in the development of THz radiation in the recent years, owing to the

[1]Department of Physics, Capital Normal University, Beijing 100048, China; [2]Beijing Key Lab of Metamaterials and Devices, and Key Laboratory of Terahertz Optoelectronics, Ministry of Education, Beijing 100048, China.

*Correspondence: Y Zhang, E-mail: yzhang@cnu.edu.cn

Received: 15 March 2022; Accepted: 17 May 2022; Published online: 4 August 2022

Open Access This article is licensed under a Creative Commons Attribution 4.0 International License.
To view a copy of this license, visit http://creativecommons.org/licenses/by/4.0/.

© The Author(s) 2022. Published by Institute of Optics and Electronics, Chinese Academy of Sciences.

fast progress of femtosecond lasers. Specifically, the energy of table-top femtosecond laser is increasing after the onset of the technology of chirped pulses amplification. There are several commonly used technologies to generate THz waves, including photoconductive antenna (PCA)[34–37], optical rectification (OR)[38–41], and plasma[42–44]. For the scheme of THz generation based on plasma, if the optical field strength is high enough to separate electrons from a media, the formed plasma will emit THz waves. Moreover, there are extraordinarily high damage threshold for the plasma scheme, which means high-energy laser pulses can be employed for THz generation. As a result, the laser-induced plasma is a more promising way to generate THz waves. It is common to group various forms of matter into distinct states, such as gas, liquid, and solid. These matters are made from atoms, which are electrically neutral. Under some conditions, such as the interaction of strong electric field of femtosecond laser pulse, these matters will be ionized to set free electrical charges and induce the plasma. With the onset of plasma, the THz wave can be radiated out. The schematic diagram of THz generation from plasma is shown in Fig. 1. Three states of matters are different in their own physical characters, leading to different scenarios of THz generations.

In this paper, we will focus on the THz generation by laser-induced plasma in gas, liquid, and solid. Since laser-plasma interactions in plasma are quite complicated, we will discuss only the various THz generation under different targets, including corresponding mechanisms and characters of the radiated THz waves, while less ionization dynamics are involved. This paper is organized as follows: In Section *THz generation from laser-induced plasma in gas*, we will introduce the THz wave generation from air plasma induced by one/two-color pulses. All the THz generation are pumped by laser pulses with the intensity lower than 10^{18} W/cm^2, at a so-called nonrelativistic level. In Sections *THz generation from laser-induced-liquid plasma* and *THz generation from laser-induced-solid plasma*, the THz generation associated with the induced plasma in liquid and solid media will be discussed, as well as their physical mechanisms and the attempts to improve the performances of the generated THz waves. Liquids will not be considered as the target to be irradiated by relativistic laser pulse. Finally, we summarize these THz generation scenarios and discuss the future development and challenges of plasma-driven THz sources in Section *Summary and outlook*.

THz generation from laser-induced plasma in gas

When femtosecond pulses propagate in optical media, a plasma will be formed as the result of ionization if the optical field strength is sufficiently intense to separate electrons. THz waves radiate from the laser-induced-air plasma. As for the involved pump optical field, the scheme of THz generation from air plasma can be divided into two parts. One is pumped by optical pulses with one central wavelength, as called one/single-color field. The other one is pumped by optical pulses with two central wavelengths, as called two-color field. The ultrafast pulses with the central wavelength of 800 nm are commonly used in the former, while the pulses with the central wavelength of 800 nm and its second harmonic of 400 nm are usually used in the latter. The physical mechanisms and characters of THz generation are different, owing to the involved pump fields.

Physical mechanisms for THz generation from laser-induced-gas plasma

THz generation from gas plasma induced by one-color pulse

As demonstrated by Hamster, the experimental condition of this THz generation scenario is quite simple that a formed plasma is enough. In this experiment, the laser pulse with the pulse width of 120 fs and energy of 50 mJ was focused to form plasma, a pulsed radiation of electromagnetic wave at THz frequency was observed

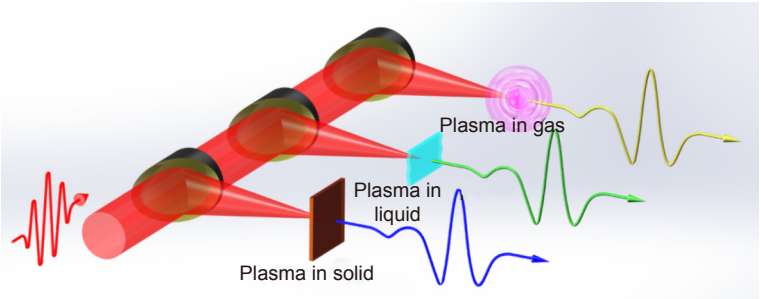

Fig. 1 | Schematic diagram of THz generation from laser-induced plasma in gas, liquid, and solid.

thereafter. Theoretically, the ponderomotive force accelerating the free electrons induces polarization, which was considered to be the mechanism of the THz generation. The ponderomotive force is described by[45–47]

$$F_{\rm pm} = -\nabla \frac{{\rm e}^2 I_{\rm opt}}{2\varepsilon_0 c m_{\rm e} \omega_{\rm opt}^2} , \tag{1}$$

here e and $m_{\rm e}$ are the charge and mass of the particle, respectively. $I_{\rm opt}$ and $\omega_{\rm opt}$ are the intensity and frequency of the femtosecond pulses. ε_0 and c are the permittivity and light speed in vacuum, respectively. The ponderomotive force model which describes the THz generation is illustrated in Fig. 2[48].

When laser pulse propagates in the air, it is subjected to the effects of diffraction, energy depletion, plasma defocusing, and nonlinear Kerr, which lead to an optical intensity gradient. The spatiotemporal optical intensity gradient causes the ponderomotive force on the electrons. The forces applied to the electrons make them to accelerate and oscillate, resulting in plasma current. The axial and transverse components of plasma current have velocities close to the group velocity of the laser pulse. The induced plasma current travels with laser pulse and emits electromagnetic pulse (EMP). That is so-called ponderomotive force model. The axial EMP electric field outside the filament is small due to shielding by surface charges at the air-plasma boundary. Note that, the characteristic frequency of the EMP measured outside of the plasma depends on the laser pulse duration and not on the local plasma frequency[48]. Technically, the ponderomotive force, radiation pressure force, as well as ionization are all included in this model.

C. Cheng presented a model to elucidate the physics underlying the THz generation from a femtosecond pulse induced plasma[49]. This so-called dipole model can be described by the process of electromagnetic emission of a diploe, in which the laser pulses spatially separate the electrons from the heavier ions to induce the dipole. The dipole moment along z-axis in the plasma channel induce the longitudinal current, which can be written as $\boldsymbol{J}(\boldsymbol{r},t) = -{\rm e}N_{\rm e}(\partial \mathcal{S}/\partial t)\boldsymbol{z}$, here $N_{\rm e}$ is the electron density and $\mathcal{S}$ is the longitudinal electron-ion separation, $\boldsymbol{r}$ is the spatial vector, $\boldsymbol{z}$ is the vector along z-axis, t is time. The current oscillating along the z-axis radiates a symmetric THz wave as

$$\left(\nabla^2 - \frac{1}{c}\frac{\partial^2}{\partial t}\right)\boldsymbol{E}_{\rm rad}(\boldsymbol{r},t) = \mu_0 \frac{\partial \boldsymbol{J}}{\partial t} , \tag{2}$$

here $\boldsymbol{E}_{\rm rad}$ is the radiated electromagnetic field, μ_0 is the permeability in vacuum. The impact of the dipole contribution to the THz generation from the plasma induced by femtosecond pulses was also investigated experimentally and theoretically[50].

In 2002, M. Kolesik presented a unidirectional optical pulse propagation equation (UPPE) to illustrate in the context of super continuum generation in the air[51,52]. In this propagation equation, various correction terms, including the linear and nonlinear terms, in the envelope approximation can be turned on or off, thus the corresponding effect can be evaluated. This model is also illustrated in the context of extreme focusing on a femtosecond pulse. The UPPE provides a seamless transition from Maxwell's equation to the various envelope-based models. These characters make the description of the EMP radiation more flexible and comprehensive. L. Berge et al. combined the UPPE and local current model and performed a lot of nice works in the THz generation induced by two-color pulse[53–56]. The unidirectional pulse propagation model for linearly polarized pulses can be written as,

$$\partial_z \boldsymbol{E} = {\rm i}\sqrt{k(\omega)^2 - k_x^2 - k_y^2}\,\boldsymbol{E} + {\rm i}\frac{\mu_0 \omega^2}{2k(\omega)}\boldsymbol{P}_{\rm NL} , \tag{3}$$

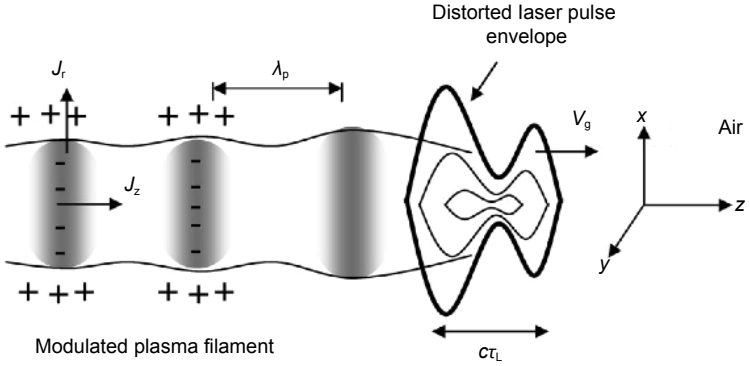

Fig. 2 | Schematic diagram of THz generation by the ponderomotive force. J_r, J_z are the radial and axial currents, respectively. λ_p is plasma wavelength. τ_L is laser pulse duration. Figure reproduced with permission from ref.[48], American Physical Society.

here $\boldsymbol{E} = \boldsymbol{E}(k_x, k_y, z, \omega)$ represents the Fourier transform, with respect to transverse coordinates and time, of the electric field. $k(\omega) = \omega n(\omega)/c$ is the wave number. The nonlinear polarization $\boldsymbol{P}_{\rm NL} = \boldsymbol{P}_{\rm Kerr} + {\rm i}\boldsymbol{J}_{\rm e}/\omega + {\rm i}\boldsymbol{J}_{\rm loss}/\omega$ originates from the Kerr effect, the electron current $J_{\rm e}$ and a photon absorption term $J_{\rm loss}$.

In 2007, D'Amico reported the generation of THz emission in the air as a new mechanism, which offers the advantages of simplicity[57,58]. In their experiment, the laser with the energy of 4 mJ per pulse, repeat rate of 10 Hz, a central wavelength of 800 nm, and a width of 150 fs has been focused in the air with a 2 m focal length lens to create a single filament. The experimental setup is shown in Fig. 3. The spectral component of the THz radiation from the plasma filament was measured by means of a heterodyne detector. The strong forward directed THz radiation was attributed from the laser induced plasma to a transition-Cherenkov emission since the electric current in the plasma moves behind the ionization front at light velocity. Compared with the Cherenkov emission, there is no net charge in the plasma and only a dipole-like structure is moving in the plasma. Additionally, the THz wave can be generated even if the velocity of the ionization front is exactly the same as the light velocity. In this model, the source term Sz is derived by the work of Spangle et al[48]. The induced current can be written as $j_z(\omega) = {\rm i}\varepsilon_0\omega E_z(\omega)$, here $E_z(\omega)$ is the field strength of plasma wave, ω is the frequency. With this current, the vector potential A will be obtained as, $A(r) = \mu_0 \dfrac{{\rm e}^{{\rm i}kr}}{4\pi r} J_{\omega,k}$, k is the field wave vector, r is radiation radius. Thus, the magnetic $B = curlA$ and the radiated electric field can be obtained by its cross product of $\mathfrak{n}$ and B.

The spectral intensity of the transition-Cherenkov emission reads as

$$\frac{{\rm d}^2 W_{\rm THz}}{{\rm d}\omega {\rm d}\Omega} = \frac{r_{\rm e} W_{\rm L}^2 \omega^2 \nu_{\rm e}^2}{16\pi^2 m_{\rm e} c^3 \omega_0^4 \theta^2} \sin^2\left[\frac{\omega L}{2c}(1-\cos\theta)\right], \quad (4)$$

here $r_{\rm e}$ is the electron classical radius, $\nu_{\rm e}$ is the electron collision frequency. $W_{\rm L}$ and $W_{\rm THz}$ are the energy of laser and THz pulses. ω_0 is the central frequency of laser pulse, L is the plasma length, Ω is the solid angle of radiation, θ is the THz radiation angle related with the laser propagation axis. One has to consider the ratio of THz wavelength over the plasma length is an important factor in this expression. With this transition-Cherenkov model, the THz radiations from a single-color filament in both time and frequency domains were investigated[50]. It was found that the plasma density, electron collision frequency, and pulse duration play important roles in the generated THz peak frequency and width of the THz spectrum.

THz generation from plasma induced by two-color pulse

In the senior of THz generation from plasma induced by one-color pulses, optics-THz conversion efficiency is lower than 10^{-7}, which cannot be used practically. However, the plasma from gas was still regarded as a promising target to radiate strong THz waves, owing to its high damage threshold and accessible phase matching in gas. Hence, the scheme of plasma induced by one-color pulses turns to two-color pulses.

In 2000, Cook and his coworkers used the femtosecond pulses with the fundamental wave (FW) and second harmonic wave (SHW) to form a plasma channel for THz waves generation[59]. They found that the

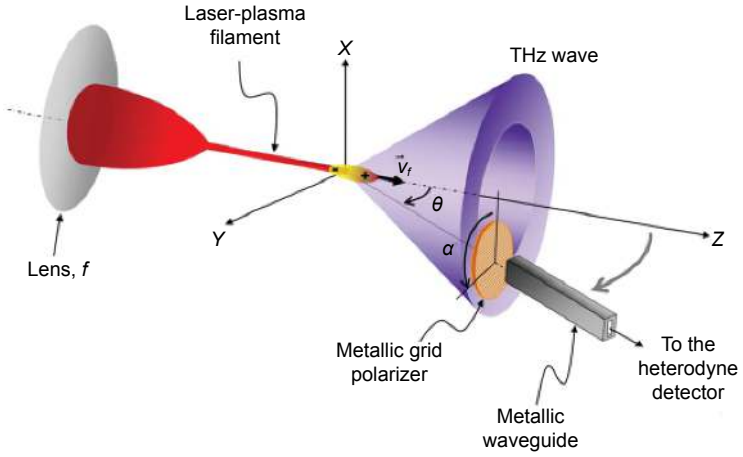

Fig. 3 | Schematic of experimental setup for measurement of THz waves from transition-Cherenkov emission. Figure reproduced with permission from ref.[57], American Physical Society.

amplitude of THz waves is surprisingly stronger than that of the plasma induced by the single-color pulse. They attributed this THz radiation to four-wave rectification (FWR), in which the third-order susceptibility was considered in the process of the radiation.

In 2004, Markus Kress measured the dependence of the THz signal on the BBO-to-focus distance[60]. As predicted from the four-wave rectification model, the maximal THz amplitude relies on the relative phase between the FW and SHW $\varphi = \omega/c(2n_{2\omega} - n_{\omega})d$, here n_{ω} and $n_{2\omega}$ are the refractive indices for FW and SHW, respectively. d is the distance between the BBO crystal to the focus. They found that the phase shift between the FW and SHW has a great impact on the generated THz signal, as shown in Fig. 4[60].

In 2006, X. Xie studied the THz generation from the plasma induced by two-color pulses through the individual control of the phase, polarization, and amplitude of the FW and SHW[61]. The measurement results show that the THz amplitude is proportionate to the intensity of FW and the square root of the intensity of SHW, as shown in Fig. 5. They attributed it as the third-order nonlinear process mixing FW and SHW in the ionized plasma, called four-wave mixing (FWM)[61]. The generated THz field can be written as

$$E_{\mathrm{THz}}(t) \propto \chi^{(3)} E_{2\omega}(t) E_{\omega}^{*}(t) E_{\omega}^{*}(t) \cos(\varphi) , \qquad (5)$$

here $E_{2\omega}$ and E_{ω} are the electric field of the SHW and FW, respectively. χ^3 is the third-order susceptibility. With this model, the experimental results can be explained well.

Initially, the proposed FWM model explained successfully the physical mechanism of THz radiation from the plasma induced by two-color pulse. However, it did not provide the microscopy origin of the nonlinearity. For

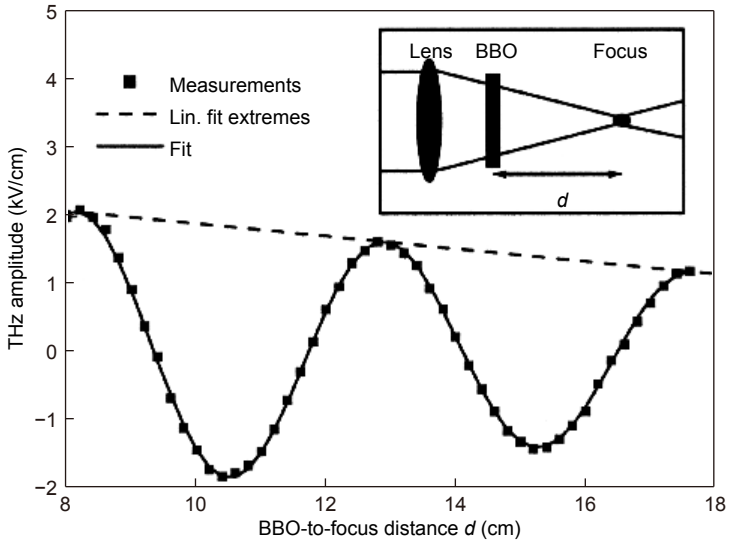

Fig. 4 | Dependence of THz signal on the phase shift between the FW and SHW. The distance of BBO-to-focus corresponds the variety of the phase shift between the two-color pulses. Figure reproduced with permission from ref.[60], The Optical Society.

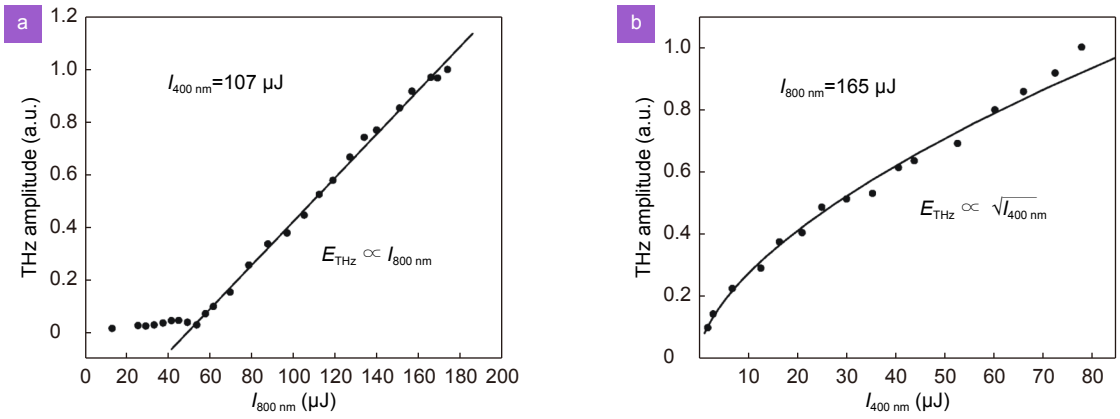

Fig. 5 | Dependence of THz field on the electric field strength of (**a**) FW and (**b**) SHW. Figure reproduced with permission from ref.[61], American Physical Society.

the same FWM model, the third –order susceptibility tensor gives different results on the THz polarization[60,62]. And then, Kim et al. proposed a plasma current model to explain the mechanism of THz generation[63,64]. Some papers have well explained the current model[53–55,65–67]. In this model, when the symmetry of the bipolarity in the total laser field is broken, an electron current arises during the ionization, and results in THz emission. The total laser field containing the FW and SHW with the same polarization can be written as

$$E_L(t) = [E_\omega \cos(\omega t) + E_{2\omega}(2\omega t + \phi)] \exp\left(\frac{-t^2}{2T_0^2}\right) , \quad (6)$$

here T_0 is the duration of FW. With two-color fields, the molecular have been ionized in air. The ionization rate can be given by

$$w(t) = 4\omega_a \left(\frac{E_a}{E_L(t)} \exp\left[\left(-\frac{2}{3}\right)\frac{E_a}{E_L(t)}\right]\right) , \quad (7)$$

here $\omega_a = (4\pi\varepsilon_0)^{-2} m_e e^4/h^3$ is the atomic frequency. $E_a = (4\pi\varepsilon_0)^{-3} m_e{}^2 e^5/h^4$ is the atomic field, h is the Planck' s constant. With the time of ionization, the increases rate of free electrons can be written as

$$\frac{dN(t)}{dt} = w(t)\,[N_0 - N(t)] , \quad (8)$$

here $N(t)$ denotes the electron density. N_0 is the initial electron density. The velocity at time t can be written as

$$v(t,t') = -\left(\frac{e}{m_e}\right)\int_{t'}^{t} dt E(t'') \exp[-\gamma(t-t'')] , \quad (9)$$

here t' is the ionization instant when the electron is born. γ is the phenomenological collision rate($\gamma \approx 5\ \mathrm{ps}^{-1}$). The electron current can be given by

$$J(t) = -\int_{\infty}^{t} e v(t,t') dN(t') , \quad (10)$$

and the generated THz field is given by

$$E_{THz} = \frac{dJ(t)}{dt} . \quad (11)$$

Recent reports reveal that both the FWM and photocurrent models work in the THz generation from the two-color induced plasma[68,69], note that plasma conversion usually prevails over Kerr response once photoionization sets in.

Characteristics of THz wave generated from laser-induce-gas plasma

Compared with the physical mechanism of THz generation from laser-induced plasma, more efforts have been put into improving the performance of THz wave, including THz amplitude/conversion efficiency, spectrum, polarization, and spatial distribution.

THz amplitude/conversion efficiency

Many attempts have been put on to enhance the THz amplitude/conversion efficiency by means of external DC electric field, length of the filament, focusing condition of the pump pulse, wavelength/harmonic component of the pump pulse, and other optical parameters of laser pulses.

Since the THz signal emitted from the plasma induced by a single-color pulse is rather weak, an external DC based electric field has been exerted on the plasma induced by a single-color pulse. The schematic of the typical experimental setup is shown in Fig. 6(a)[70]. In this work, a model based on transition-Cherenkov was used to explain the experimental results. When an external DC based electric field was brought to the ionized plasma region along direction X, the current leading to THz wave can be written as

$$J_\omega = \frac{\varepsilon_0 E_s \omega_{pe}^2}{\omega^2 - \omega_{pe}^2 + i\nu_e\omega} , \quad (12)$$

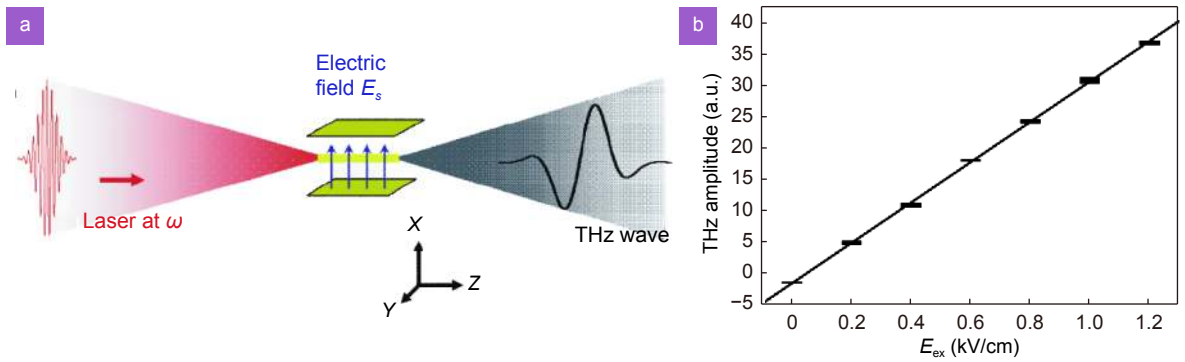

Fig. 6 | (**a**) Schematic of experimental setup for THz generation based on external electric fields in single color plasma and (**b**) experimental results. Figure reproduced with permission from: (a) ref.[70], American Physical Society; (b) ref.[71], The Optical Society.

here, ω_{pe} is the plasma frequency, E_s is the external statistic electric field. With this relation, this model predicts a relation of the radiated THz energy to the applied field as

$$W_{THz} \approx \frac{\pi}{8}\varepsilon_0 E_s^2 r_0^4 L \frac{\omega_{pe}^3}{c^2 \nu_e}\ , \tag{13}$$

here, r_0 is the radius of plasma. The enhancement of THz is also considered as a result of the increase of second harmonic current when there is an external DC electric field in the plasma region[71]. With this increased second harmonic current, the enhanced THz wave was explained via the magnetic vector potential and scalar potential. In the experiment, above 1000-fold enhancement of the radiated THz energy has been observed, when a static electric field exerting on the plasma. The experimental results are shown in Fig. 6(b). Additionally, there are other electric fields exerting technology and theoretical explanations for this THz generation from the DC based plasma[72–74].

Since the laser beam is focused to form a plasma which emits THz waves, the number of filaments has been considered as a way to increase the energy of the output THz waves. Two filaments[75–77] or even filament array[78,79] have been formed in the experiments with the technology of coherent syntheses. The radiated THz wave is about 1 order of magnitude more intense than that from a single-filament under the same experimental condition.

It is noted that the length of the plasma can modify the THz field generated from the two-color pulse induced plasma, in which the filamentation process was tailored[80]. Therefore, the approaches of increasing the length of plasma to increase the THz signal have also been investigated[81–84]. In their experiments, they observed that THz amplitude increased with the length of the plasma channel.

It is well known that the plasma can be formed by focusing laser pulses. Therefore, the focusing conditions were considered for getting intense THz radiation. K. Liu et al. demonstrated that a 5.3-time enhanced THz pulse energy was observed when the plasma was formed by abruptly autofocusing laser beam[85]. The feedback wave front was manipulated to get the best focus to enhance the THz radiation, in which a 6 folds improvement was obtained[86]. A cylindrical lens was used to focus the femtosecond pulse to avoid plasma-induced laser defocusing and subsequent THz saturation[87]. The results showed that the energy conversion efficiency is of 7×10^{-4}, about 7 times better than the spherical lens focusing. In addition, there are other reports about the contribution of the focusing condition on the THz radiation enhancement[88–91].

The parameters of the femtosecond pulse are important factors to be used in increasing the energy of THz radiation. Conventionally, pulses of the FW at 800 nm and SHW at 400 nm are used to induce plasma and emit THz wave. In the scheme of THz generation from the plasma induced by two-color pulse, the electric current obtains a drift velocity that scales linearly with the wavelength of laser pulse ($\nu_d \propto \lambda$). It was reported that the THz energy scales as $\propto \lambda^2$ or $\propto \lambda^{4.6}$. A. Nguyen et al. reported THz energy scaling like λ_0^a with large exponents $5.6 \leq a \leq 14.3$, which departs from the growth in λ^2 expected from photocurrent theory[56]. Although the scales are not coincident, the results show that a longer laser wavelength is desirable to get higher energy. Efficient THz generation from air plasma via mid-infrared coherent control has been investigated experimentally and theoretically[92–95]. In 2020, it was demonstrated that two-color plasma induced by femtosecond mid-infrared laser pulse at 3.9 μm can generate THz wave with sub-mJ energy and the THz conversion efficiency is about 2.36%[96]. The record of 2.36% is partly due to the change of pump polarization. Using the circularly-polarized two-color pulse can increase the THz energy yield[97,98]. Another possibility for increasing THz yield is to increase the number of colors[65,67,99]. The harmonic component involved in the formation of plasma is also an important factor for the enhancement of THz generation[100–102]. It was shown experimentally that the efficient THz occurs at the condition of new rations of $\omega_2/\omega_1 = 1:4$ or $2:3$, which are the uncommon frequency ratios in the two-color scheme[103] can be achieved. Chirped pulse[104,105] and carrier-envelope phase[106,107] are also the parameters of femtosecond pulses to enhance the THz energy.

THz spectrum

As described above, the THz signal generated from air plasma induced by one-color pulse is rather weak, leading to a low signal noise ratio (SNR). Accordingly, its Fourier-transformed spectrum is with low SNR too. To demonstrate the spectrum of THz wave generated from plasma induced by one-color pulse, the external electric field was applied in the plasma region[70]. In the experiment, the THz signal was characterized by a plasma-based

technology[108,109]. The results are shown in Fig. 7(a). It can be seen that the SNR in the THz spectrum is still quite low although an external electric field is exerted on the plasma region. It also shows that the bandwidth of the spectrum spans to ~10 THz. Moreover, the spectrum of THz wave generated from air plasma induced by two-color pulse was also measured. In the experiment, the THz spectrum was measured by Fourier-transform infrared spectrometry. The result is shown in Fig. 7(b)[110]. It can be found that the THz spectrum spans to ~20 THz with a higher SNR. Though different detection methods were used in characterizing the spectrum of THz wave generated from air plasma, the results show that under the same experimental conditions the spectrum of THz wave generated from air plasma is wider than that from other optics-to-THz methods, which may be owing to the lack of quantum absorption in air plasma. Additionally, the results show that the spectrum of THz wave generated from plasma induced by two-color pulse is wider than that by the one-color one.

Usually, a formed plasma emits THz pulses with a fixed spectrum, modulated THz spectrum may provide more potential applications. Many attempts have been tried to modify the profile distribution of the radiated THz spectrum[111–113]. As an easy and practicable way, the temporal coherence of THz pulses has been considered to be utilized in modifying the output THz spectrum[114]. In experiments, the THz waves were generated by two optical paths, in which the femtosecond pulses were controlled to induce plasma separately. By adjusting the time delay between the pulses in two paths, the superposition of THz waves generated in two paths resulted in modulated spectra. After that, the wavefront of the femtosecond pulse was controlled by the method of inserting a fixed phase plate, which subsequently manipulated the profile distribution of the radiated THz spectrum[80]. Recently, Y. Zhang reported a simple and energy-saving method for actively modulating the output THz waves spectrum with a liquid crystal spatial light modulator (LC-SLM)[115]. The LC-SLM actively controls the wavefront of femtosecond pulses and facilitates the replacement of the fixed phase plate. The schematic of the experimental setup and results are shown in Fig. 8. In the experiment, two focuses are formed and adjusted by the phase distribution on the SLM to induce two serial plasmas with spatiotemporal intervals. With this proposed method, the modulation of THz spectrum has been observed and the amplitude dip has been manipulated, as shown in Fig. 8(b). Filamentary gratings have also been demonstrated as a frequency modulator[116]. Additionally, the spectrum of THz radiation can also be controlled by tailoring two-color laser beams[117].

Polarization

Polarization of THz radiation emitted from plasma has been initially investigated in the aspect of measurement and characterization. In 2007, D'Amico observed that the plasma induced by single-color pulse emits radially polarized THz waves[57], as shown in Fig. 9. In the measurement, a metallic grid polarizer was used to detect the polarization of emitted THz waves. From the figure, it can be found that the radiated THz wave is radially polarized. The radial polarization has also been observed in ref.[118]. So far, the radial polarization of THz radiation from plasma induced by a single-color pulse is universally accepted.

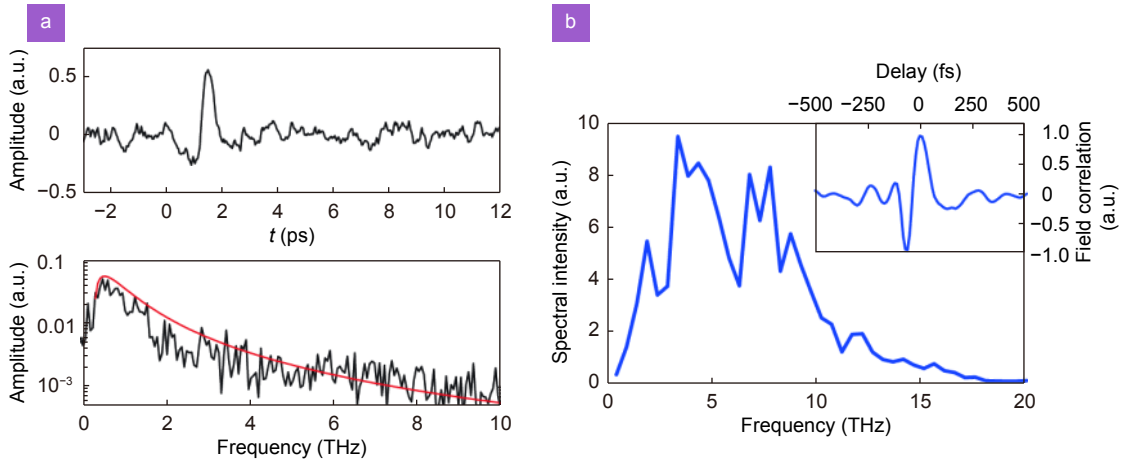

Fig. 7 | THz signals generated from air plasma induced by (**a**) one-color pulse and (**b**) two-color pulse. Simulation result is shown by the red line in (a). Figure reproduced with permission from: (a) ref.[70], American Physical Society; (b) ref.[110], under a Creative Commons Attribution licence.

For the case of THz wave from plasma induced by two-color pulse, the process of condition is rather complicated. In 2009, the polarization of THz waves from plasma induced by two-color pulse has been investigated experimentally and theoretically[119]. It was shown that the polarization of THz wave is linear when both the pulses of FW and SHW are linear polarized. The THz radiation generated by circularly-polarized pump waves (FW and SHW) with the same helicity may be observed not linearly polarized in the experiment, which is out of the expectation of plane wave theory. It owns to the spatial alignment and non-collinear propagation of the two-color pulses[98]. The mechanism of elliptically polarized THz wave generation in femtosecond two-color induced plasma has also been investigated[120–122]. After that, the research on the polarization of THz radiation from the two-color pulse induced plasma has been turned to controlling[123–125]. Various polarization of THz wave can be realized via modifying the polarization of laser pulse or external electric field. By exerting a helical electric field on the plasma region, an elliptically polarized THz signal was observed[126]. By using a cross-DC biasing approach, the polarization of THz waves can be freely varied from linear to elliptic with arbitrary ellipticity[127]. By individually controlling the polarization of the pulses of FW and SHW beams, the plasma induced by two-color pulses can also emit THz signal with linear-to-elliptical polarization[128]. By inducing the circularly polarized femtosecond pulse to form plasma, elliptically polarized THz waves radiation have been observed[129].

Spatiotemporal distribution

Great efforts have been put into the investigation of the spatial distribution of THz wave generated from the laser induced plasma. For the scenario of single-color, the spatial distribution is commonly believed to be conical. But in the case of two-color, the spatial distribution may be rather various, including bell-shape, conical shape, and ring-shape. In the early time of the exploration, the observed results mostly depend on the detection methods used in the experiments, including line scanning, raster scanning, and CCD array detecting.

H. Zhong induced the technology of line-scanning into heterodyne detection of THz waves[130]. In the experiment, a metal slit with a width of 2 mm was moved vertically in a plane before the lens. Combining with the technology of electro-optical (EO) sampling, the angle distribution of the THz radiation was measured. The

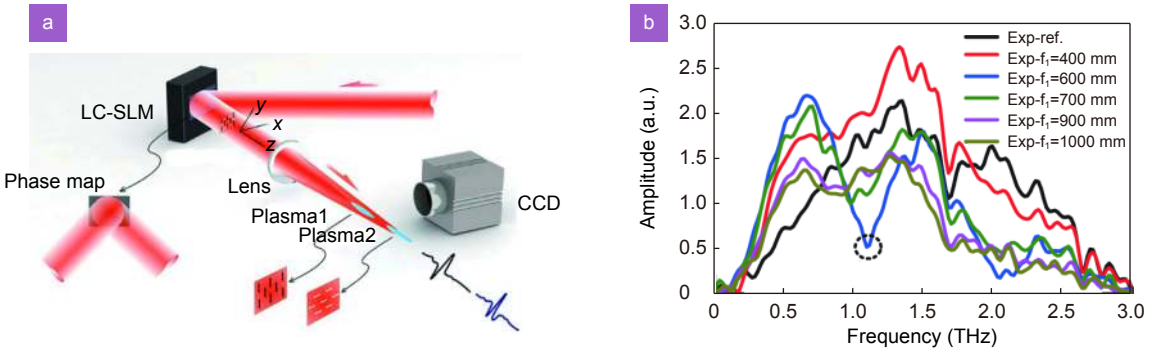

Fig. 8 | (**a**) Schematic of the experimental setup and (**b**) results of actively modulated THz spectra. Figure reproduced with permission from ref.[115], The Optical Society.

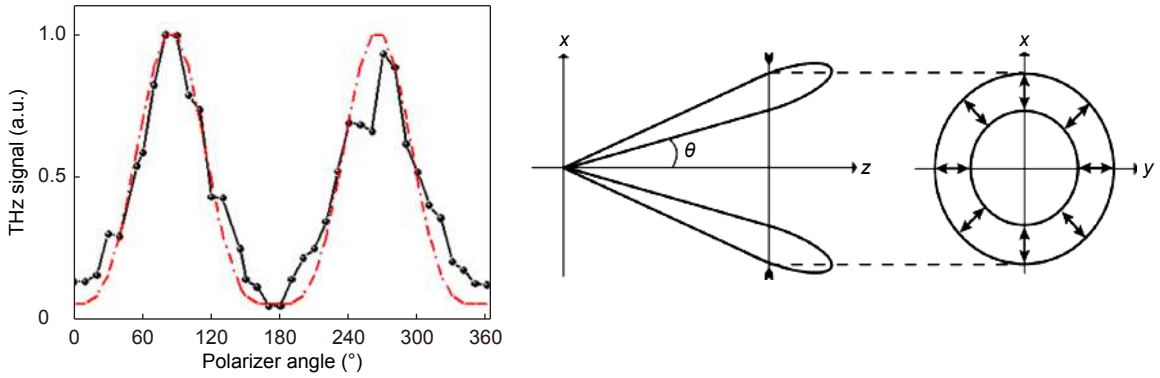

Fig. 9 | Polarization of THz forward emission measured at θ = 10°. The experimental and simulation THz signals are denoted with black and red dots. Figure reproduced with permission from: ref.[57], American Physical Society.

experimental result shows that the THz intensity profile in the cross section is a Gauss-like type. The angle distribution of THz generation from laser induced plasma was also measured by the technology of line scanning and Michelson interferometer[68]. The measurement for the frequency-angle spectra of THz radiation was performed by moving a 1.5 mm slit across the diverging THz beam. The measured angle distribution of THz wave exhibits a maximum at about 4°~6° relative to the propagation axis. The off-axis maximum in the angle distribution corresponds to a ring-shape. At the same time, the experimental result was simulated by the non-propagating plasma fluid model. Both the experimental and simulation results show that 15% of the THz energy propagates on the axis and 85% in the region of ring.

The technology of line scanning is easily operated and time-saving, but if this technology is used in the measurement of the spatial distribution, the obtained results cannot reveal the real THz spatiotemporal distribution, because the obtained signal is the integration of the unblocked individual signal values. In 2009, with the technology of raster-scanning, R. A. Akhmedzhanov measured the spatial distribution of THz radiation from two-color pulse induced plasma[131]. In the experiment, the spatial distribution was scanned by moving a field stop in a transverse plane. The obtained intensity distribution is bell-shaped. It was explained by the self-phase modulation of a laser pulse with high intensity propagating in a plasma. The spatial distribution of THz radiation from two-color pulse induced plasma was also investigated by a raster scanning pyroelectric detector[132]. In the experiment, a silicon wafer is used to filter out the unwanted optical and infrared light. Filters were used to characterize THz profiles at different frequency bands. The measured far field THz profiles are donut-shaped, as shown in Fig. 10. In this work, the dephasing length is about 22 mm. As shown in Fig. 10(a), the plasma length is shorter than the dephasing length, so that all THz waves constructive interference in the forward direction, concentrating THz radiation on axis. Fig. 10(a) and 10(b) are from a plasma with the length of 10 mm, 10(c) and 10(d) are from a plasma with the length of 40 mm. 10(e) and 10(f) are simulated THz profiles for a plasma with the length of 40 mm. 10(a) and 10(c) show the profiles of THz waves at low frequency owing to a Teflon filter, while 10(b) and 10(d) show the profiles of THz waves at high frequency owing to a germanium filter. All figures show that the far-field THz radiation profiles are doughnut–shape in the THz frequency range. Additionally, an off-axis phase matched model was utilized to simulate the radiated THz spatial distributions. The doughnut-shaped distribution of THz radiation from two-color pulse induced plasma by the technology of raster scanning was also demonstrated in ref.[133]. Compared with the technology of line-scanning, the raster-scanning technology is more accurate in obtaining the THz spatial distribution. The accuracy of the measurement depends on the size of the stop. The small size will lead to more accuracy measurement results under the same experimental

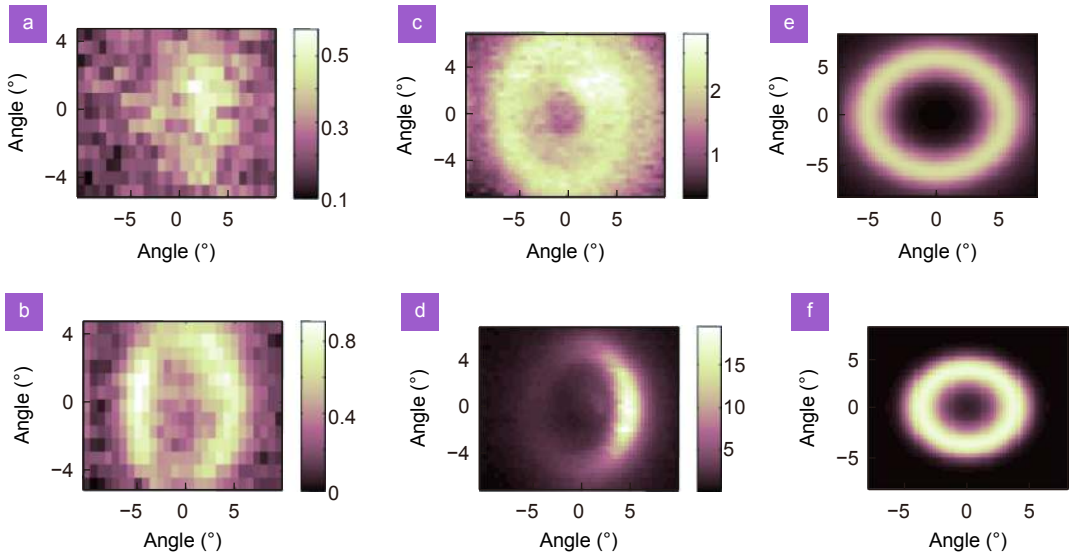

Fig. 10 | Measured and simulated far-field THz radiation profiles. Experimental results (**a**–**d**) were obtained by raster scanning of a pyroelectric detector with a silicon filter. (**a**) and (**b**) are from a plasma with the length of 10 mm. (**c**) and (**d**) are from a plasma with the length of 40 mm. (a) (c) Teflon and (b) (d) germanium filters are used for low and high frequency transmission. (**e**) and (**f**) are simulated THz profiles for a plasma with the length of 40 mm. Figure reproduced with permission from ref.[132], American Physical Society.

condition. However, if the size of the stop approaches mm or sub-mm, the diffraction effect will be obvious, resulting in errors in the measurement. Additionally, the raster scanning technology is time-consuming, which is a challenge to the stability of the experimental system.

In 2014, a THz camera with the bandwidth of 1–7 THz was used to capture the THz intensity profile[134]. The recorded THz images are shown in Fig. 11. In the unfocused intensity profile shown in Fig. 11(a), it can be found that the THz intensity pattern in the far-field is in the form of a donut-shaped profile, and it evolves into a spot after being focused, as shown in Fig. 11(b). With the series of intensity profile images recorded by THz camera, a 3D THz profile has been obtained. Recently, with the technology of THz focal-plane imaging[135,136], E. L. Wang measured the spatiotemporal distribution of THz radiation from two-color pulse induced plasma[137]. Compared with the above imaging technologies, the THz focal-plane imaging technology can provide more detailed information on THz images, including amplitude, phase, frequency, and even polarization. The schematic of the experimental setup is shown in Fig. 12. It is clear that the spatiotemporal distribution varies with the frequency as well as the length of plasma. A donut-shaped profile occurs in the lower THz frequency range. The results are shown in Fig. 13. Moreover, the length of plasma channel, focusing condition, pulse duration, or even the filter are important factors contributing to the spatial distribution of THz radiation[138–140].

THz generation from laser-induced-liquid plasma

Liquid water as a target to generate THz waves has been historically considered to be impossible owing to its significant absorption in the THz band[141]. Like the gas media, the fluidity of liquids makes it replenish quickly, which leads to a high damage threshold in the liquid target when it was irradiated by intense laser pulses. However, compared with the gas media, the liquid target has more than 3 orders of molecular equivalent cross section[142]. The above characters make it reasonable to expect the liquid to be a candidate for intense THz sources. In 2017, the broadband THz radiation from the plasma in liquid water has been experimentally demonstrated, which was also induced by femtosecond laser pulse[143]. After that, various experiments with different liquids and geometries have been investigated.

Physical mechanism for THz generation from laser induced liquid plasma

THz generation from liquid plasma induced by single-color pulse

Understanding the physical mechanism for THz

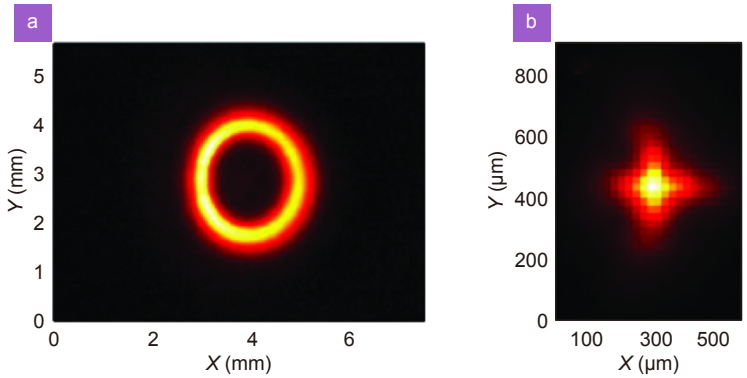

Fig. 11 | Intensity image recorded by a THz camera. (**a**) Unfocused THz intensity profile and (**b**) focused intensity THz profile. Figure reproduced with permission from ref.[134], under a Creative Commons Attribution (CC BY) licence.

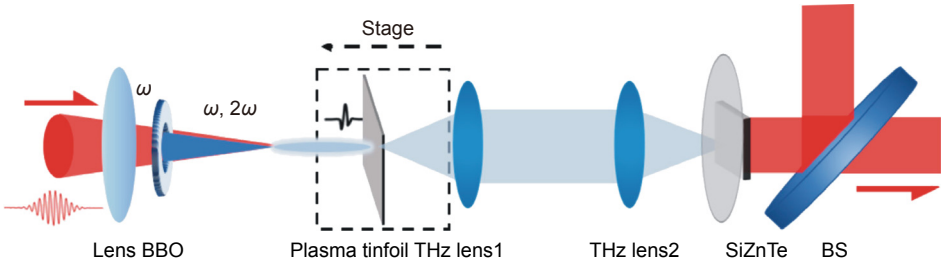

Fig. 12 | Schematic diagram of experimental setup for THz focal-plane imaging. Figure reproduced with permission from ref.[137], under a Creative Commons Attribution 4.0 International License.

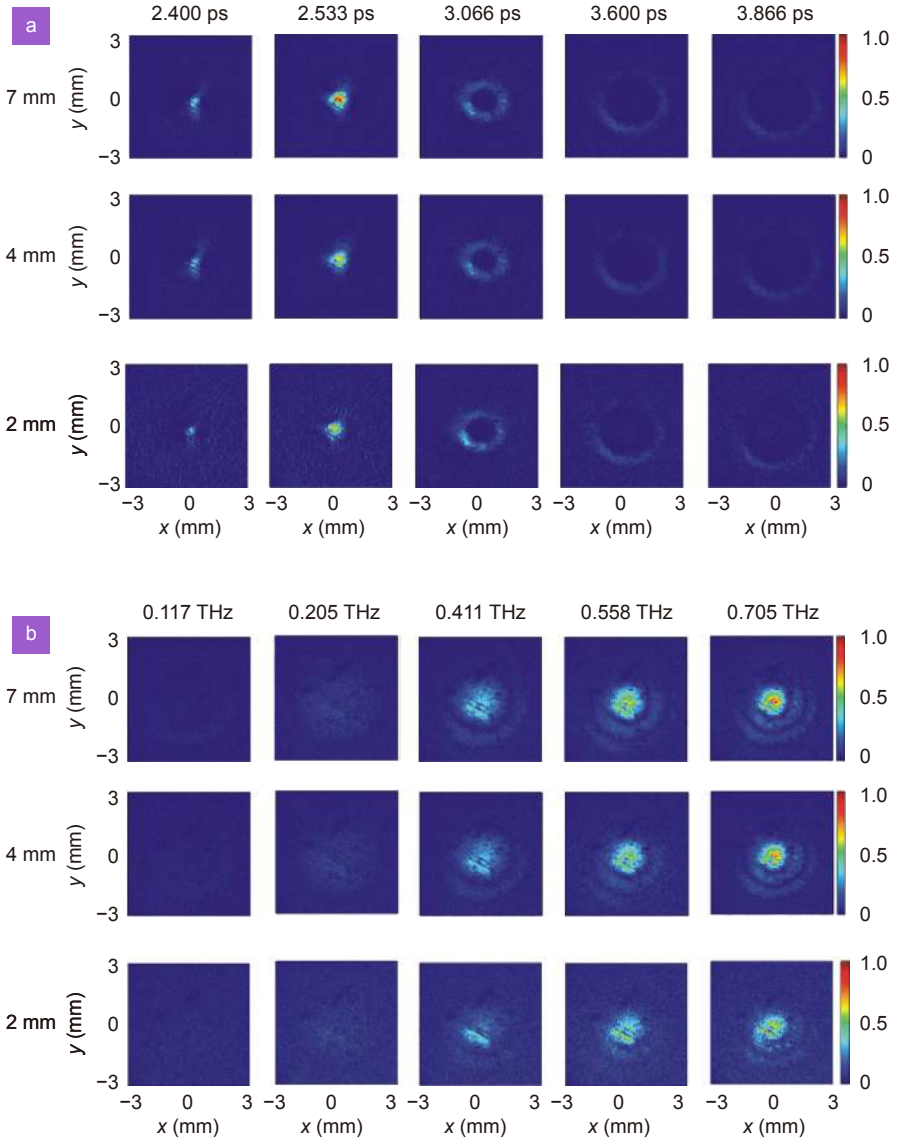

Fig. 13 | Intensity distributions of THz waves generated from plasmas with different lengths. THz images in the (**a**) time domain and (**b**) frequency domain. Figure reproduced with permission from ref.[137], under a Creative Commons Attribution 4.0 International License.

generation from liquid target is essential for advancing THz aqueous sources. A diploe model based on the ponderomotive force is proposed to explain the THz generation from laser-induced liquid plasma[144]. A schematic of the dipole model, which shows the schematic diagram of the THz radiation process, is shown in Fig. 14. The laser pulse penetrates and is refracted at the air/water interface of the water film, and then ionizes water molecules at the focus. In the ionized region, the quasi-free electrons move towards the regions of lower electron density with the ponderomotive force. The ions keep relatively stationary owing to the relatively large mass. The density of ionized carriers keeps identical in the forward direction for the reason that the envelope of the laser pulse faster than the electron. Therefore, the electrons are accelerated backward, leading to a dipole structure and emitting THz waves. The THz intensity can be described as

$$I_{\mathrm{THz}}(\alpha,\beta) \sim T_1(\alpha)\, T_2(\beta) \sin^2[\gamma(\alpha,\beta)] \times \exp\left(-\frac{a_{\mathrm{pTHz}} d_{\mathrm{f}}}{2\cos\theta_{\mathrm{t}}(\beta)}\right)\left(\frac{W_{\mathrm{L}}}{r_0}\right)^2, \quad (14)$$

here α is the incident angle of laser pulse. β is the detection angle of THz wave. T_1 and T_2 are transmittance of the laser pulse and THz wave. γ is the measurement angle related to the direction of the dipole. θ_{t} is the exiting angle of THz waves. a_{pTHz} is the absorption coefficient of THz waves. W_{L} is the energy of laser pulse, and d_{f} is the thickness of water film. With this model, THz intensities are simulated and normalized. As shown in

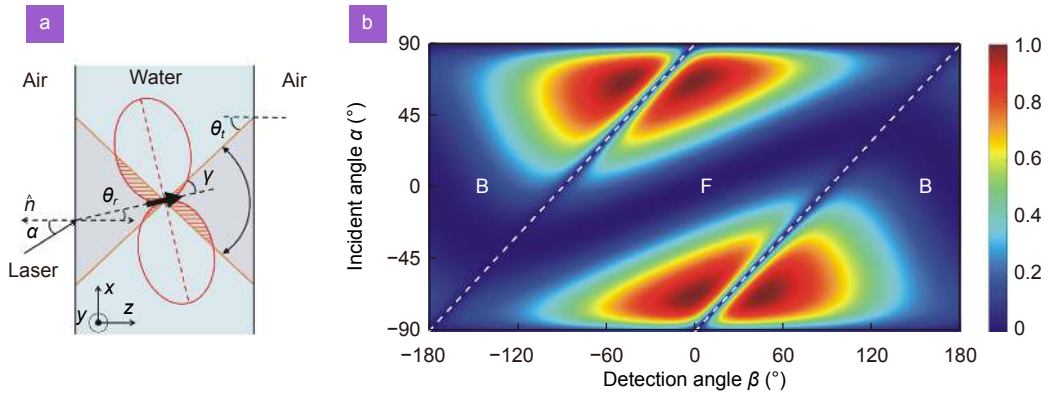

Fig. 14 | Ponderomotive force–induced dipole model for THz generation from liquid water. (**a**) Schematic diagram of the diploe model for THz generation from the plasma in the water film. (**b**) Its simulation result. α, θ_r are the incidence and refractive angle for the laser pulse, β and θ_t are the detective angle and exiting angle for THz pulse. F and B indicate the forward and back propagation THz signals, respectively. Figure reproduced with permission from ref.[144], AIP Publishing.

Fig. 14(b), F and B indicate the forward and back propagation of THz signals, respectively. The symmetric pattern results from the symmetric structure geometry in the model. The simulation results support the observation of the THz intensity dependence on the laser incident angle.

In 2020, a two-dimensional dipole array model was introduced to illustrate the THz wave emission from water line[145]. In this model, the THz emission is considered as superposition of emission by a 2D dipole array, and expressed by

$$E_{\text{array}} = E(1 + \mathrm{e}^{\mathrm{i}kd\sin\theta} + \mathrm{e}^{2\mathrm{i}kd\sin\theta} + \cdots), \tag{15}$$

here E is the THz electric field generated from each dipole in the array. θ is the angle between the observation point and the spherical coordinate axis. d is the distance between two adjacent dipoles. With this model, the dependence of THz peak electric field on the relative positional relation between the plasma and the water line was simulated. The simulation result agrees well with the experimental one.

In 2019, the mechanism of laser ponderomotive-force-induced current with the symmetry broken around the water-column interface was attributed to the THz generation from a liquid water line[146]. In this model, the THz radiation was considered to originate from a net current owing to the presence of the column interfaces. The currents distribute on two sides of the laser propagation axis, which were formed by the ponderomotive force. If the laser axis deviates from the water column center, the symmetry of the two currents will be broken. The generated THz electric field can be written as

$$E_{\text{THz}} \sim \frac{W_{\text{L}} N_{\text{e}}}{w_0^2}, \tag{16}$$

where w_0 is the width of the laser beam. This model implies THz strength scales linearly with the laser energy.

A theoretical model which describes the physics of ultrashort pulses has also been used in the THz generation from liquid water[147,148]. In this model, the dynamics of the radiation field, the evolution of the current density of quasi-free electrons, and the dynamics of the concentration of electrons have been included,

$$\begin{aligned}
&\frac{\partial E}{\partial z} + \Gamma_0 E - a_{\text{p}}\frac{\partial^3 E}{\partial \tau^3} + gE^2\frac{\partial E}{\partial \tau} + \frac{2\pi}{cn_0}j = 0\ ,\\
&\frac{\partial j}{\partial \tau} + \frac{j}{\tau_{\text{c}}} = \xi\rho E^3\ ,\\
&\frac{\partial \rho}{\partial \tau} + \frac{\rho}{\tau_{\text{p}}} = \zeta E^2\ ,
\end{aligned} \tag{17}$$

where Γ_0, a_{p}, and n_0 are the empirical coefficients characterizing the dependencies of the medium absorption and the refractive index. g characterizes the low-inertia cubic nonlinear response of the medium, j is a current density of quasi-free plasma electrons. ρ is excited states population of the medium molecules. τ_{c} and τ_{p} are times of relaxation from quasi-free and excited states. ζ and ξ are the efficiency of the transitions to the above states. z is the position of propagation. The schematic and simulation results of this model are shown in Fig. 15. The pump laser pulse propagates in the liquid and ionizes the liquid via multiphoton absorption. With the formation of the plasma channel, THz waves radiate in both directions, as shown in Fig. 15(a). The THz energy versus the pump pulse duration and liquid thickness was simulated, as the result shown in Fig. 15(b). For clarity, some typical data were abstracted from Fig. 15(b) to compare with the experimental ones. Both the experimental and simulation results show that the maximum generation efficiency of THz radiation varies with the liquid thickness

and the pump pulse duration. With this model, the quasi-quadratic dependence of THz energy on the optical excitation has been revealed. Certainly, as a theoretical description via equations, the UPPE is also used to describe the THz generation from laser-induced liquid plasma[149], which was utilized in the scenario of THz generation from air plasma.

A unified model from the principle of electrodynamics was induced to explain both single/two color excitation of THz waves from a liquid[150]. In this model, both the ponderomotive force along the laser propagation axis and the drift current perpendicular to the laser propagation axis have been considered. The schematic diagram is shown in Fig. 16. The generated THz field can be logically written as

$$E_{\mathrm{THz}}(t) \propto N_{\mathrm{e}} a_{\mathrm{p}}(t) + \frac{\partial N_{\mathrm{eT}}(t)}{\partial t} v_{\mathrm{d}}(t) \ , \qquad (18)$$

where a_{p} is the acceleration from the ponderomotive force, v_{d} is the drift velocity of electrons under an asymmetric field composed of the FW and SHW. The first term on the right-hand side is relative to the acceleration from the ponderomotive force, while the second one corresponds to the drift motion of newly generated electrons. With this model, the THz generation from the water film was well explained.

Properties of THz wave generated from laser-induced liquid plasma

Great efforts have been put into the improving the properties of THz wave generated from laser-induced plasma in liquid. Like the case of the air, different liquids and excitation geometries have been investigated for the excitation. THz intensity, spectrum, and polarization are also included in the concerned properties of the liquid sources.

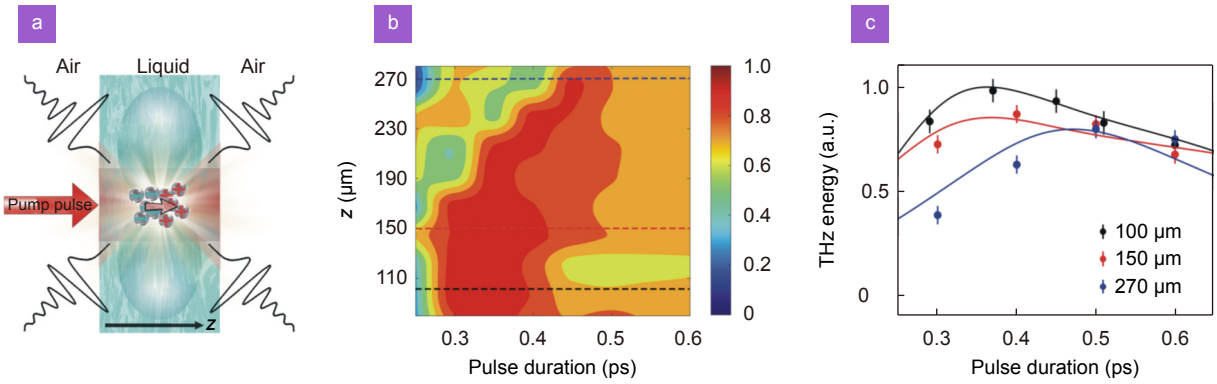

Fig. 15 | Model of ultrashort pulses propagation equation and its simulation results. (**a**) Visualization of the model description, (**b**) simulation result of THz signal with different liquid thickness and pump pulse duration, and (**c**) comparison of experiment results with simulated results abstracted from (b). Figure reproduced with permission from ref.[147], The Optical Society.

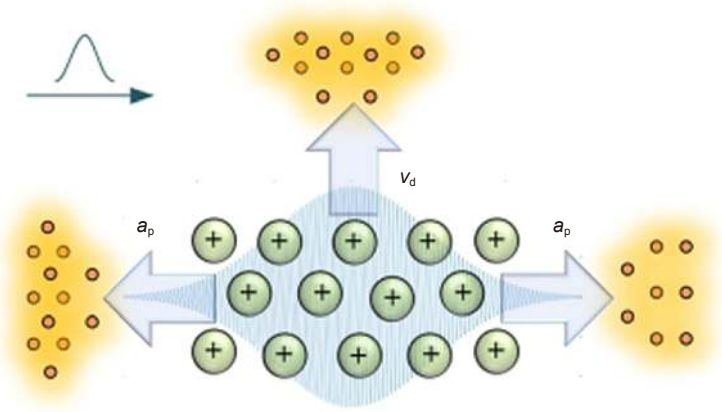

Fig. 16 | Schematic diagram of the particle dynamics in the unified theoretical model. a_{p} and v_{d} are the acceleration and drift velocity of electrons, respectively. They are related to the laser propagation direction and electron dynamics in the water medium. The electrons are accelerated forward and backward between the ascending and descending edges owing to the ponderomotive force. v_{d} is perpendicular to the laser propagation direction. The combined effect of a_{p} and v_{d} results in THz generation in liquid water. Figure reproduced with permission from ref.[150], AIP Publishing.

THz intensity

To get intense THz wave from liquid, the crucial factors affected THz generation, including the optimal angle of optical incidence, optimal pulse duration for optical excitation, and geometry parameters of liquid, have been investigated.

Optimal angle of optical incidence. The dependence of THz intensity on the incidence angle of optical pulses was measured in the experiment of excitation of liquid water films, the results are shown in Fig. 17. The blue dots and black squares denote the data measured by a Golay cell and EO sampling, while the red line denotes the simulation results. B and F represent the back and forward propagation signals. It is clear that the optimal incidence angle is independent of the water thickness. Apart from it, about ~80% of energy is dissipated when $\alpha = 65°$, due to the total internal reflection at the surface and the absorption of water. It can be found that the optimal angle of optical incidence is 65°, which was owing to the results of the transmittance of the p-polarized excitation laser at the air/water interface and the dipole direction. A similar result is also observed when a water line is used as a THz source. In these experiments, the optimal incidence angel depends on the asymmetry optical excitation, project of dipole component in x direction and total internal reflection of THz wave at the liquid/air interface[144,145].

Optimal pulse duration of optical excitation. In the case of THz generation from air plasma, the dependence of THz amplitude on the laser pulse duration has been explored in many works[54,151]. It is found that the THz amplitude increases with the increasing of the laser pulse duration at low laser intensity, while decreasing with the increasing laser pulse at a high laser intensity, in which the ionization events play an important role[151]. This dependence was also explored in the case of THz generation from liquid plasma. It was observed that from either water film or line, the optimal pulse duration for THz wave generation is in the order of sub-picosecond[143,147,148,152]. This observation results from the dependence of plasma formation in water on the optical pulse duration, in which the electron density (corresponding to the pulse width) plays an important role[153].

Geometry parameters of liquid. The diameter of the water line is also considered in the contribution to the generated THz signal. It was demonstrated that the strongest THz wave generates when the diameter of the water line is in the range of 0.1–0.2 mm[145,152]. The preference of the diameter range was simulated by the model of electromagnetic wave propagation equations, and it was attributed to the changed pulse duration in water, which results in the enhanced THz signal[153].

Energy of laser pulse. The dependence of THz electric field strength on the energy of laser pulse has also been investigated. In most of the experiments, the linear dependence of THz intensity on the energy of laser pulse was observed before the saturation of THz signal[144,146]. However, there are measurements revealing that the THz energy scales quasi-quadratically with the optical pulse energy[146,147,154]. The difference of the observed dependence may result from the liquid target geometry and the excitation energy of the laser pulse. It is noted that the THz energy generated for the single-color induced plasma in liquid is more than that in air, given it under the same experimental conditions.

Spectrum

The spectrum of THz wave generated from liquid plasma

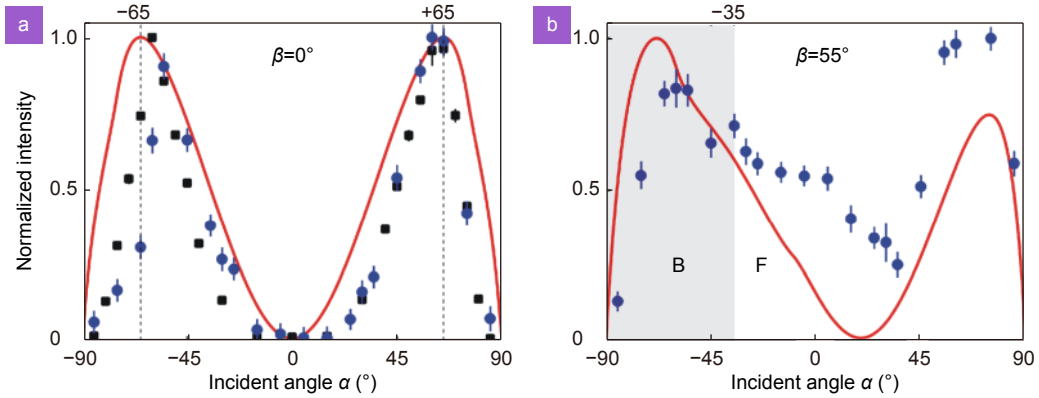

Fig. 17 | THz intensity versus incidence angle α for different detection angle β, (**a**) β = 0° and (**b**) β = 55°. The blue dots and black squares denote the data measured by a Golay cell and EO sampling, while the red line denotes the simulation results. F and B represent the forward and back propagation signals. Figure reproduced with permission from ref.[144], AIP Publishing.

was characterized by Fourier-transformed time domain signal. It was found that the bandwidth of THz wave is narrower than that of air plasma (tens THz)[155,156]. It shows that there is an obvious diversity in the frequency component profile of the THz wave, where the high frequency is more than that of the low frequency, as shown in Fig. 18. When the pulse width increases from 50 fs to 300 fs, the difference of spectrum characters becomes inconspicuous. This inconspicuous difference results from the decreased energy of SHW pulse at a longer duration, which make the effect of SHW pulse insignificant.

Apart from the water, other liquids have been used as the target in the THz generation from liquid plasma, such as α-pinene, *p*-xylene, and ethanol[147,153]. The spectra of THz waves generated from α-pinene and water are shown in Fig. 19. It is clear that the spectrum of THz waves generated from α-pinene has more high-frequency components and a wider bandwidth. The refractive index and absorption of α-pinene are contributed to the difference and shown in the inset. Besides that, the material-related function in the ionization process is also a contributor to the discrepancy. THz spectra width has been specially investigated with different liquid targets[149]. It shows that 99.5% of the spectral power lies between 0.1–50 THz for air, 72% and 64% of the spectral power for acetone and ethanol, respectively.

Polarization

For the THz generation from liquid plasma, the effort on THz polarization is not so much as the case of air plasma. Further exploration on polarization is limited, maybe owing to the complicated configuration and geometry. Only one experimental and theoretical investigation showed that the THz wave is always p polarized whether the optical exciting pulse is s or p polarized[146].

THz generation from laser-induced-solid plasma

Intense THz radiation is always pursued due to its numerous applications. As described above, overcoming the damaged problem make plasma a promising medium to produce THz radiation. However, the way to further enhance the THz yield by increasing the pump laser intensity is always blocked. The saturation of the ionization current will occur if the laser intensity is up to $\sim 10^{15}$ W/cm^2. Currently, the peak intensity of an ultra-intensity laser pulse can be above 10^{18} W/cm^2, which is commonly called relativistic laser[157,158]. At this level, the electron quiver velocity in the laser field approaches the light speed. Under this experimental condition, the plasma without saturated ionization current from a target is desirable.

Compared with the media of air and liquid, a higher density of electron can be obtained from the plasmas of solids. Furthermore, the solids can endure the higher intensity of laser pulse. Hamster et al. observed the THz emission from aluminum thin foils with the pump laser pulses at relativistic intensity $\sim 10^{19}$ W/cm^2 [159,160]. At present, intense THz pulses with energy up to tens of mJ have been observed from the relativistic laser pumping solid targets. There is no evidence showing the saturation of THz signal even the pump intensity is up to 10^{20} W/cm^2 [161]. Although intense THz wave can be obtained in the way of relativistic laser-solid interaction, the involved mechanisms are rather complicated and are still in exploration.

Physical mechanisms for THz generation from laser-induced-solid plasma

THz generation from plasma wave

When the laser pulse propagates in the plasma, its

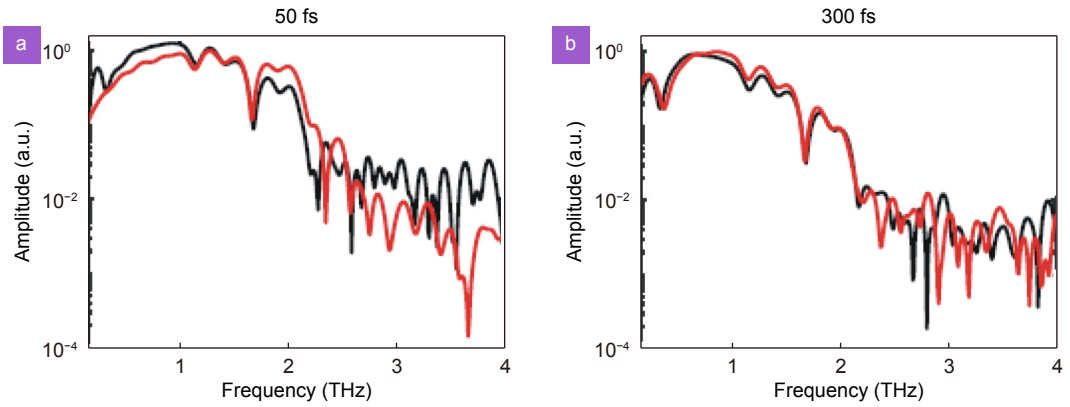

Fig. 18 | Spectra of THz waves generated from a 120 μm thick water film with one-color (black line) and two-color (red line) excitation schemes in the case of the pulse duration of (**a**) 50 fs and (**b**) 300 fs. Figure reproduced with permission from ref.[155,156], AIP Publishing.

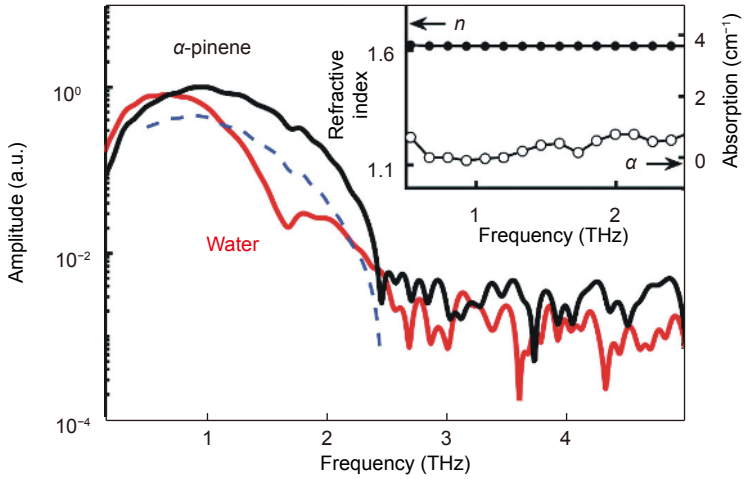

Fig. 19 | Spectra of THz waves generated from *α*-pinene and water. Figure reproduced with permission from ref.[153], under a Creative Commons Attribution 4.0 Unported License.

energy is coupled to the plasma via resonant absorption. In this process, a plasma wave with a large amplitude is excited, also called as laser wakefield. This electrostatic plasma wave happens at the critical density where the frequencies of plasma and laser are nearly equivalent. This electrostatic plasma wave can be reversed to electromagnetic wave if some conditions are required[162]. In unmagnetized plasma, the dispersion relations for the electrostatic and electromagnetic wave are expressed as $\omega = \omega_p^2 + 3k^2v_e^2$ and $\omega = \omega_p^2 + k^2c^2$, respectively. It is obvious that the electrostatic wave can be efficiently converted to the electromagnetic with the conditions k=0 and $\omega = \omega_p$, as illustrated in Fig. 20(a)[163]. In the plasma with homogenous density, the wave number of the electrostatic wave $k = \omega_p/v_g \neq 0$, ω_p and v_g are the frequency of plasma and group velocity of laser. Hence the linear conversion cannot occur in the plasma with homogenous density. In the plasma with inhomogeneous density, the wave number of electric static varies with its spatiotemporal distribution, which makes it possible to convert the electric static wave into the electromagnetic wave. Apart from the condition of k=0, the incidence angle of the laser to the inhomogeneous plasma must be considered.

The electrostatic wave is a longitudinal wave, while the electromagnetic wave is a transverse one. If they propagate in the same direction, the linear conversion cannot occur. Thereafter, when the intense laser pulse irradiates obliquely to an inhomogeneous plasma with under density, the projected components of both electric fields are partially in parallel. The THz wave can be emitted from the electrostatic wave in the specular reflection direction. Liao et al. observed the intense THz radiation generated from plasma wave[165]. Based on this theory, the observation was explained by the excitation via the stimulated Raman scattering and self-modulated laser wakefields.

In the magnetized plasma, the transverse motion of the electron is formed by the Lorenz force and induces a transverse current, which makes the magnetized wakefields convert partially into the electromagnetic wave, with a frequency closer to the frequency of plasma, which is commonly called Cherenkov wake radiation[164]. The geometry of the external B field compared with the propagation axis of the exciting source is illustrated in Fig. 20(b).

THz generation from electron transport

When the pump laser intensity is above 10^{18} W/cm^2, the typical density of the induced plasma can arrive 10^{17}/cm^3. In this scenario, the intense laser can break the wakefield oscillation, which leads the wakefield-based emission mechanism will not work[166]. When the relativistic laser irradiates on the solid target, the electron generated in the laser-plasma interaction will be accelerated and transported in a short time scale, which produced a time-varying transient current to radiate electromagnetic waves. This radiation is believed to be responsible for the radiation in the infrared and THz spectra range. The electron transports in longitudinal and lateral directions. If a relativistic laser pulse interacts with an over dense plasma from the solid target, the joint contribution of light pressure and electrostatic restore force creates the longitudinal motion of bunches of electrons, and radiates intense THz pulse[167]. Apart from the longitudinal electron transport, the lateral transport has also been

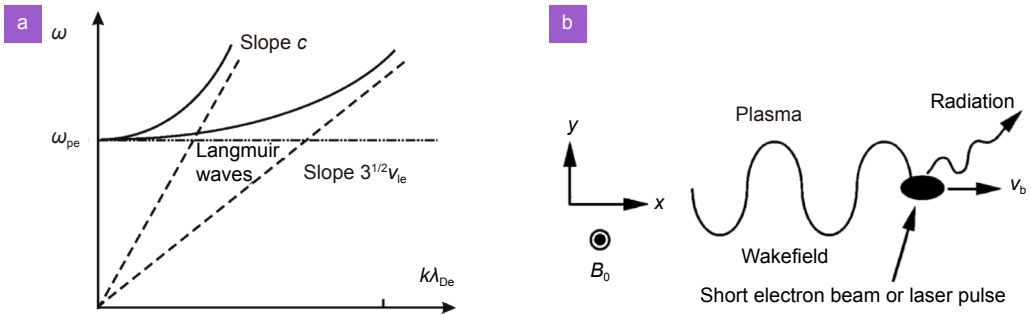

Fig. 20 | (**a**) Dispersion curves of plasma waves and electromagnetic waves and (**b**) Cerenkov wake radiation. v_b is the velocity of the disturbance that creates the wake in the medium. Figure reproduced with permission from: (a) ref.[163], IEEE; (b) ref.[164], American Physical Society.

observed[168,169]. In the experiment, the longitudinal transport was excluded because it exists in the high-density region and THz wave cannot escape from this region. The lateral current has been validated by the 2D particle-in-cell simulation, which is informed by electrons propagating near the target surface owing to the confinement of the spontaneous quasi-static magnetic and electrostatic fields at the surface[170,171]. In the simulation, the p-polarized laser pulses irradiate on the front target surface at an incidence angle of 60° as shown in Fig. 21(a), the density of the plasma slab is 6 nC, where nC is the critical density. Thus, there is a surface current at the vacuum-plasma interface along the *y*-direction at time of 50, 60, and 70 laser cycles, as shown in Fig. 21. It can also be found that the current flows in the *y*-direction with time. Consequently, the lateral electron transport is contributed to the THz radiation. With this mechanism, a self-organized fast electron current model is proposed to explain the observations.

When laser pulses are irradiated on a solid target with a moderate density gradient at a small incidence angle, the emitted THz waves show different features[172]. Two types of transient current driven by either the laser ponderomotive force or two-plasmon decay (TPD) have been analyzed. The experimental results of TPD are shown in Fig. 22. In the experiment, a laser pulse at the wavelength of 800 nm was used to irradiate the target, the spectrum of the scattered light contains $3/2\omega_0$ and $2\omega_0$ components as shown in the upper-left inset of the figure, where ω_0 is the laser frequency. When the laser contrasts are changed, the THz energy is independent of the $2\omega_0$ component, as shown in another inset of the figure. During this THz radiation, the THz energy scales linearly with the intensity of $3/2\omega_0$ signal. Since the $3/2\omega_0$ component is an indicator for TPD instability, the transient current included by TPD is determined via the $3/2\omega_0$ component. The results show that the transit current induced by TPD is responsible for the observations. With the theory of lateral transport of electron, the radiation energy with frequency was also explained[173].

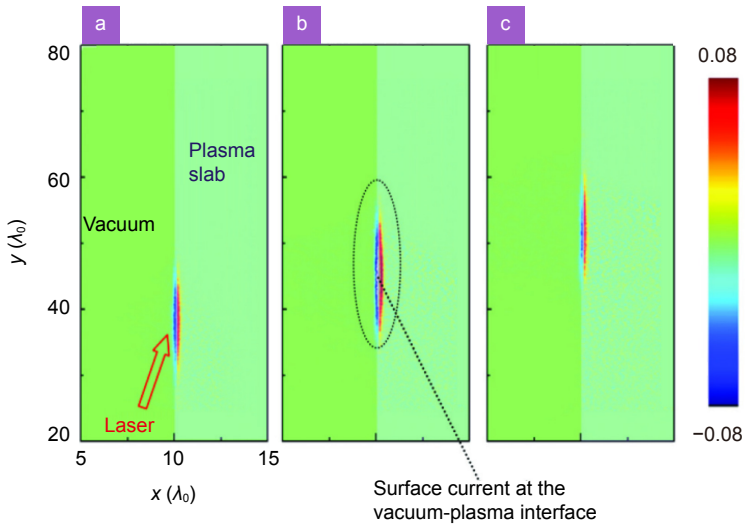

Fig. 21 | Electron current distributions at the surface of solid target obtained from 2D particle-in-cell simulations. (**a**), (**b**), and (**c**) are the cases at the time of 50, 60, and 70 laser cycles, respectively. Figure reproduced with permission from ref.[169], AIP Publishing.

THz generation from plasma emission

When the relativistic laser pulse is irradiated on the solid target, there is a scenario that THz radiation is emitted from the target rear surface. For the case of THz radiation from the target front surface, it is a result of the direct interaction of the NIR laser pulse with the foil, where the surface current is formed by the motion of electrons from the plasma. However, in the case of THz generation from the target rear surface, the THz dynamics are different. There are mainly two mechanisms involved in the dynamics, coherent transition radiation (CTR) and sheath radiation (SR).

Transition radiation is produced by an electron bunch passing through a metal foil. The electron was accelerated by the laser wakefield to have enough kinetic energy to escape the target. When the electrons transit the plasma-vacuum boundary, they will induce a lateral polarization current owing to the dielectric discontinuity[172,174]. This current gives rise to the THz radiation. The THz radiation induced by one electron is weak. However, during the transition radiation, the electron bunch length is in the order of 10 μm and shorter than the emitted THz wavelength. According to the relation of the bunch structure with the radiation wavelength[175,176], the transition radiation from the electron bunches becomes coherent, with a power proportional to the square of the number of electrons. The CTR process is illustrated in Fig. 23(a).

As the electrons escaping the target surface, a strong charge separation field with the behavior like a dipole is formed owing to the electron dynamics. The separation field is comparable to the peak electric field of the laser pulse, and accelerates the positive protons to a very high energy, resulting in electromagnetic emission. Because the evolution time scale of the separation field is in the order of picoseconds[177], the emitted electromagnetic waves are in THz band. The THz field is correlated with the square of the numbers of protons. This is so called target sheath acceleration (TNSA), as illustrated in Fig. 23(b). In order to form a quasi-static field accelerating ions over ps time scales, the sheath radiation needs the go and back motions of less energetic electrons from the rear of the target.

There are many more complicated physical processes are involved in the relativistic laser-solid interaction, especially in the case of submicron solid target. By analyzing the fields emitted by longitudinal and transverse currents, J. Dechard et al. reveals that the THz emission consists of CTR and antenna-type emission, in which the first one results the recirculation hot electrons, while the second one results from the shielding of electron currents[178].

Characteristics enhancement for THz wave generated from laser-induced solid plasma

THz intensity

As expected, the scheme of laser-solid interactions can provide intense THz waves, the focus of this scheme is mostly on the THz enhancement. By optimizing the preplasma scale length, extremely broadband THz bursts with energy of above 100 μJ/sr in the laser specular was observed[165]. For the CTR, energetic electron bunch with both high charge density (nC-μC) and short duration (fs-ps) will provide high THz radiation energy. The THz

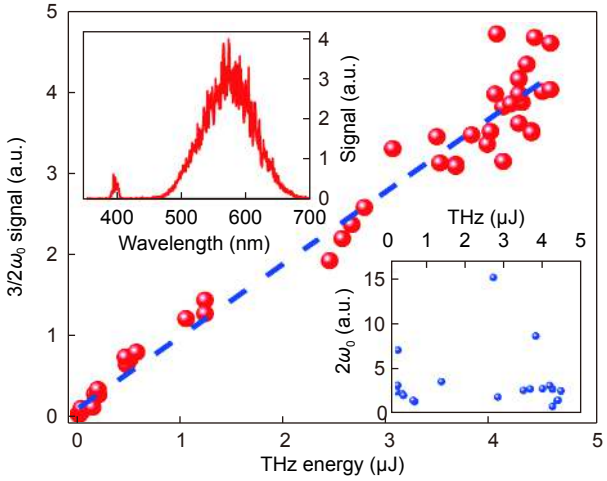

Fig. 22 | Relation of the 3/2ω_0 signal intensity of the scattered light with the THz energy. Figure reproduced with permission from ref.[172], AIP Publishing.

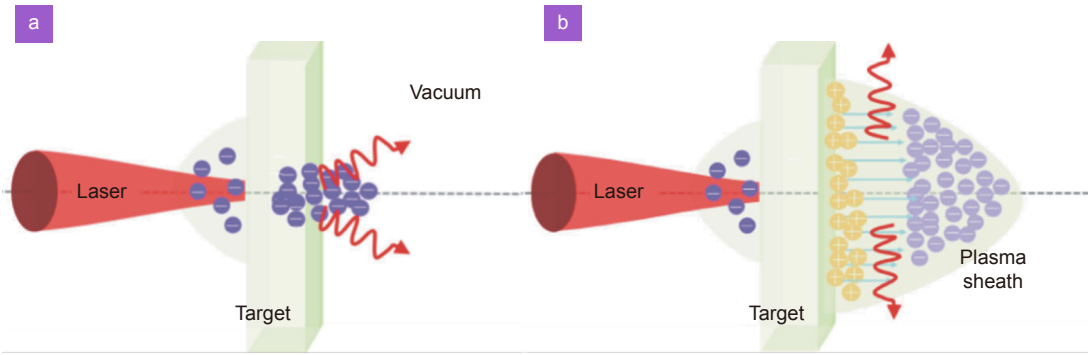

Fig. 23 | Schematic diagrams of two main mechanisms for THz generation from plasma emission. (**a**) Coherent transition radiation and (**b**) sheath radiation. Figure reproduced with permission from ref.[175], under a Creative Commons Attribution (CC BY) licence.

energy about 3~5 nJ over a collection angle of 30 mrad was experimentally demonstrated when the 1.5 nC electron bunch was used[179]. It is predicted that the THz energy will be enhanced to mJ-level by increasing the energy of electron beam and the transverse size of plasma[180,181]. By irradiating the foil targets with femtosecond or picoseconds laser pulses, the THz energy of ~400 μJ and ~50 mJ have been demonstrated experimentally[182,183].

For the TNSA, the THz pulses with energy of 460 μJ have been observed experimentally at the rear surface of a thin metal foil[176]. Target structure is also considered to enhance the THz energy via increasing the laser absorption. It is predicated that the targets with gratings or multilayer structure can emit more THz energy than a flat target[184]. This structured target was used in the experiment, in which 10-fold of enhancement of THz energy has been observed from a thick planar target with deposited copper nanorod arrays[185].

Spectrum

By changing the parameters of plasma and laser pulse, the backward THz radiation from solid targets in the presence of the preplasmas has been widely investigated[169,172,173,186,187]. The results show that the low-frequency radiation will emit under the conditions of a larger laser incidence angle and a steep plasma density at the target surface, while the high-frequency one corresponds to the conditions of a smaller incidence angle and a moderate plasma density.

Polarization

The polarization of THz pulse from the laser-solid interaction is still in exploration. Radially polarized THz pulse has been observed from the rear surface of a thin foil irradiated by laser pulse[176,188]. By focusing radially polarized THz fields from the laser-irradiated thin foil, longitudinal polarized THz pulse has been observed[189].

Summary and outlook

In this paper, the focus is mainly on an overview of mechanisms and properties concerning the generation of THz radiation from laser-induced plasma in air, liquid, and solid. For the scenarios of THz generation from laser-induced plasma in air and liquid, only the cases of pump laser pulse in the nonrelativistic region are involved. For the scenario of THz generation from laser-induced plasma in solid, only the cases of the irradiated laser pulse in the relativistic region are involved. There are some cases excluded in this paper, such as pumping liquid nitrogen, metal (Hg, Ga) and pumping air with relativistic laser pulses. There are many significant works on the relativistic interaction to THz energy yields from air plasma[190,191], and they are not reviewed in detail owing to the length limitation of this paper. For the mechanisms of THz generation from the laser induced plasma are overviewed, it was divided according to the pump laser fields, as one/two color. Since THz generation from laser-induced plasma is an increasingly active research field, it is inevitable to cover all relevant reported mechanism in this paper. For the properties of THz generation from laser-induced plasma in three medias, the THz energy/efficiency, spectrum/bandwidth, polarization, and angular distribution are reviewed separately in corresponding sections. A comparison of THz generation from laser-induced plasma in three media is shown in Table 1.

In terms of THz generation from laser-induced plasma in gas, its THz signal is larger than that from the effect of optical rectification of crystals, which is commonly used in the THz time domain spectroscopy. However, the SNR is worse than that of the effect of optical rectification of crystal. Hence, the performance of SNR should be improved. The spectrum of THz radiation from the laser-induced-air-plasma can be

broadened to ~100 THz, thus, it is frequently used in the ultrabroad absorption spectrum measurement of a sample. However, the solution and bandwidth of the spectrum depending on the detection method. Therefore, both the performance of SNR and detection method should be addressed for its wide applications. It is well known that the two-color scheme of THz radiation from laser-induced plasma in the air is very popular to generate THz waves in labs. Its mechanisms and corresponding boundaries of validity are still in exploration. If they are established, it will help to deepen the understanding of the physics of THz generation from plasma. It is well known that the wavelength of THz is shorter than that of MW, leading to its advance of imaging resolution. However, the conical THz radiation form laser-induced plasma in gas characters a hollow distribution in the far-field. The hollow distribution may be modified by reshaping the THz pulse, or controlling the wavefront of laser pulse to directly generate THz wave with solid-core distribution.

In terms of THz generation from laser-induced plasma in liquid, its plasma density is higher than that from the gas which induces a higher THz signal than that from gas with the same condition of pump laser power. However, the THz field is not scaled with the electron density. It is out of expectation and maybe owing to the absorption of THz waves by liquids. Unlike a string plasma induced in gas, the length of plasma induced in liquid is rather short, meaning the number of electrons contributed to THz yield is not much. Therefore, increasing the length or volume of induced-liquid-plasma and decreasing the absorption of THz wave are important for enhancement of THz wave in the scheme of liquid. For the corresponding mechanisms, most of theoretical models are based on plasma in the gas. It is known that there are many differences in the dynamics of liquid and gas. Therefore, innovative theories on these mechanisms are expected, which will help to understand the physics in depth. Compared with the THz generation from gas and solid, the THz generation from liquid is rather new, and the obtained results are not sufficient. The justification of the models may depend on the further research results. As described in the section of THz generation from laser induced plasma in gas, many attempts have been put on increasing the THz yield or broadening its spectrum, including modifying target geometry, pumping with different wavelength of laser pulse, external electrical field, and controlling the electron density and dynamics. These attempts can also be applied on the scenario of THz generated from laser-induced plasma in liquid.

In terms of THz generation from laser-induced plasma in solid, energetic THz waves are always generated from the solid plasma. However, the samples were excited by laser pulse in single-shot mode, meaning refreshment of solid target after each shot. The output THz efficiency is limited by the degradation of the solid target. Therefore, replenishing of energetic electrons is required to match the repeat rate of the exciting laser pulse. As described above, the electron bunch charge and bunch duration limit the THz peak power. Hence, one can expect energetic electric bunch (nC-μC) and short bunch duration (fs-ps) to get high peak power THz waves. As a new THz source, the THz radiation from the laser-induced plasma in solid is still in exploration. The validated mechanisms and tunable properties including spectrum, polarization, and angular distribution will be feasible.

In terms of the applications of THz radiated from the laser-induced plasma in three medias, it always drives the investigation going further and into depth. Since THz waves are directly from the plasma, they could serve

Table 1 | Comparison of THz generation from laser-induced plasma in gas, liquid, and solid.

	Gas	Liquid	Solid
Configuration	Atmosphere	Film, line, droplet	Foil, bulk
Laser excitation intensity	Nonrelativistic	Nonrelativistic	Relativistic, >10^{18} W/cm^2
Excitation field	One/two-color	One/two-color	One-color
THz field	>100 MV/cm[96]	~MV/cm[149]	~0.8 GV/cm[183]
Conversion efficiency	2.36%[96]	>0.1%[149]	~0.1%[183]
THz energy	0.185 mJ[96]	76 μJ [149]	~2.3 mJ[183]
THz bandwidth	>50 THz[96]	~100 THz[149]	<20 THz[183]
Geometry	Easy	Complicated	Complicated
Laser pulse width	~fs	~ps	fs-ps
Detective THz yield	Forward/sideway	Forward/sideway	Forward/sideway/backward

as a useful diagnostic tool for the plasma wave, particle acceleration, and transport of electron during the formation of plasma. Since the THz fields generated from laser induced plasma in three medias are prevailing over other THz sources, there is ample scope for its abilities in the extreme THz science, especially the interaction of strong THz field and matter. It also plays important roles in the pump/probe technology, in which the THz wave can be employed to induce structural response of a sample. In addition, their distinctive applications should be in practice, for example, THz generation from laser induced plasma in the air is greatly expected to be used in the remote sensing, in which the propagation of THz wave is replaced with that of laser pulse to avoid the absorption of THz wave.

References

1. Cocker TL, Jelic V, Gupta M, Molesky SJ, Burgess JAJ et al. An ultrafast terahertz scanning tunnelling microscope. *Nat Photonics* **7**, 620–625 (2013).
2. Ho IC, Guo XY, Zhang XC. Design and performance of reflective terahertz air-biased-coherent-detection for time-domain spectroscopy. *Opt Express* **18**, 2872–2883 (2010).
3. Turner GM, Beard MC, Schmuttenmaer CA. Carrier localization and cooling in dye-sensitized nanocrystalline titanium dioxide. *J Phys Chem B* **106**, 11716–11719 (2002).
4. Leitner DM, Havenith M, Gruebele M. Biomolecule large-amplitude motion and solvation dynamics: modelling and probes from THz to X-rays. *Int Rev Phys Chem* **25**, 553–582 (2006).
5. Niessen KA, Xu MY, Markelz AG. Terahertz optical measurements of correlated motions with possible allosteric function. *Biophys Rev* **7**, 201–216 (2015).
6. Williams MRC, Aschaffenburg DJ, Ofori-Okai BK, Schmuttenmaer CA. Intermolecular vibrations in hydrophobic amino acid crystals: experiments and calculations. *J Phys Chem B* **117**, 10444–10461 (2013).
7. Bergé L, Kaltenecker K, Engelbrecht S, Nguyen A, Skupin S et al. Terahertz spectroscopy from air plasmas created by two-color femtosecond laser pulses: the ALTESSE project. *Europhys Lett* **126**, 24001 (2019).
8. Henry SC, Zurk LM, Schecklman S, Duncan DD. Three-dimensional broadband terahertz synthetic aperture imaging. *Opt Eng* **51**, 091603 (2012).
9. Zanotto L, Piccoli R, Dong J L, Morandotti R, Razzari L. Single-pixel terahertz imaging: a review. *Opto-Electron Adv* **3**, 200012 (2020).
10. Guo LH, Wang XK, Han P, Sun WF, Feng SF et al. Observation of dehydration dynamics in biological tissues with terahertz digital holography [Invited]. *Appl Opt* **56**, F173–F178 (2017).
11. Ducournau G, Szriftgiser P, Beck A, Bacquet D, Pavanello F et al. Ultrawide-bandwidth single-channel 0.4-THz wireless link combining broadband quasi-optic photomixer and coherent detection. *IEEE Trans Terahertz Sci Technol* **4**, 328–337 (2014).
12. Koenig S, Lopez-Diaz D, Antes J, Boes F, Henneberger R et al. Wireless sub-THz communication system with high data rate. *Nat Photonics* **7**, 977–981 (2013).
13. Nagatsuma T, Horiguchi S, Minamikata Y, Yoshimizu Y, Hisatake S et al. Terahertz wireless communications based on photonics technologies. *Opt Express* **21**, 23736–23747 (2013).
14. Nicoletti D, Cavalleri A. Nonlinear light–matter interaction at terahertz frequencies. *Adv Opt Photonics* **8**, 401–464 (2016).
15. Hafez HA, Chai X, Ibrahim A, Mondal S, Férachou D et al. Intense terahertz radiation and their applications. *J Opt* **18**, 093004 (2016).
16. Mittleman DM. Perspective: terahertz science and technology. *J Appl Phys* **122**, 230901 (2017).
17. Hwang HY, Fleischer S, Brandt NC, Perkins Jr BG, Liu MK et al. A review of non-linear terahertz spectroscopy with ultrashort tabletop-laser pulses. *J Mod Opt* **62**, 1447–1479 (2015).
18. Novelli F, Ruiz Pestana L, Bennett KC, Sebastiani F, Adams EM et al. Strong anisotropy in liquid water upon librational excitation using terahertz laser fields. *J Phys Chem B* **124**, 4989–5001 (2020).
19. Zalden P, Song LW, Wu XJ, Huang HY, Ahr F et al. Molecular polarizability anisotropy of liquid water revealed by terahertz-induced transient orientation. *Nat Commun* **9**, 2142 (2018).
20. Sajadi M, Wolf M, Kampfrath T. Transient birefringence of liquids induced by terahertz electric-field torque on permanent molecular dipoles. *Nat Commun* **8**, 14963 (2017).
21. Bodrov S, Sergeev Y, Murzanev A, Stepanov A. Terahertz induced optical birefringence in polar and nonpolar liquids. *J Chem Phys* **147**, 084507 (2017).
22. Tcypkin A, Zhukova M, Melnik M, Vorontsova I, Kulya M et al. Giant third-order nonlinear response of liquids at terahertz frequencies. *Phys Rev Appl* **15**, 054009 (2021).
23. Rasekh P, Safari A, Yildirim M, Bhardwaj R, Ménard JM et al. Terahertz nonlinear spectroscopy of water vapor. *ACS Photonics* **8**, 1683–1688 (2021).
24. Kampfrath T, Tanaka K, Nelson KA. Resonant and nonresonant control over matter and light by intense terahertz transients. *Nat Photonics* **7**, 680–690 (2013).
25. Novelli F, Guchhait B, Havenith M. Towards intense THz spectroscopy on water: characterization of optical rectification by GaP, OH1, and DSTMS at OPA wavelengths. *Materials* **13**, 1311 (2020).
26. Olejnik K, Seifert T, Kašpar Z, Novák V, Wadley P et al. Terahertz electrical writing speed in an antiferromagnetic memory. *Sci Adv* **4**, eaar3566 (2018).
27. Schlauderer S, Lange C, Baierl S, Ebnet T, Schmid CP et al. Temporal and spectral fingerprints of ultrafast all-coherent spin switching. *Nature* **569**, 383–387 (2019).
28. Pálfalvi L, Fülöp JA, Tóth G, Hebling J. Evanescent-wave proton postaccelerator driven by intense THz pulse. *Phys Rev ST Accel Beams* **17**, 031301 (2014).
29. Nova TF, Cartella A, Cantaluppi A, Först M, Bossini D et al. An effective magnetic field from optically driven phonons. *Nat Phys* **13**, 132–136 (2017).
30. Nanni EA, Huang WR, Hong KH, Ravi K, Fallahi A et al. Terahertz-driven linear electron acceleration. *Nat Commun* **6**, 8486 (2015).
31. Zhang XC, Shkurinov A, Zhang Y. Extreme terahertz science. *Nat Photonics* **11**, 16–18 (2017).
32. Li X, Qiu T, Zhang JH, Baldini E, Lu J et al. Terahertz field–

induced ferroelectricity in quantum paraelectric $SrTiO_3$. *Science* **364**, 1079–1082 (2019).
33. Vella A, Houard J, Arnoldi L, Tang MC, Boudant M et al. High-resolution terahertz-driven atom probe tomography. *Sci Adv* **7**, eabd7259 (2021).
34. Dreyhaupt A, Winnerl S, Dekorsy T, Helm M. High-intensity terahertz radiation from a microstructured large-area photoconductor. *Appl Phys Lett* **86**, 121114 (2005).
35. Beck M, Schäfer H, Klatt G, Demsar J, Winnerl S et al. Impulsive terahertz radiation with high electric fields from an amplifier-driven large-area photoconductive antenna. *Opt Express* **18**, 9251–9257 (2010).
36. Tong M Y, Hu Y Z, Xie X N, Zhu X G, Wang Z Y et al. Helicity-dependent THz emission induced by ultrafast spin photocurrent in nod-al-line semimetal candidate Mg_3Bi_2. *Opto-Electron Adv* **3**, 200023 (2020).
37. Imafuji O, Singh BP, Hirose Y, Fukushima Y, Takigawa S. High power subterahertz electromagnetic wave radiation from GaN photoconductive switch. *Appl Phys Lett* **91**, 071112 (2007).
38. Blanchard F, Razzari L, Bandulet HC, Sharma G, Morandotti R et al. Generation of 1.5 μJ single-cycle terahertz pulses by optical rectification from a large aperture ZnTe crystal. *Opt Express* **15**, 13212–13220 (2007).
39. Carnio BN, Schunemann PG, Zawilski KT, Elezzabi AY. Generation of broadband terahertz pulses via optical rectification in a chalcopyrite $CdSiP_2$ crystal. *Opt Lett* **42**, 3920–3923 (2017).
40. Blanchard F, Schmidt BE, Ropagnol X, Thiré N, Ozaki T et al. Terahertz pulse generation from bulk GaAs by a tilted-pulse-front excitation at 1.8 *μ*m. *Appl Phys Lett* **105**, 241106 (2014).
41. Hauri CP, Ruchert C, Vicario C, Ardana F. Strong-field single-cycle THz pulses generated in an organic crystal. *Appl Phys Lett* **99**, 161116 (2011).
42. Zhang ZL, Zhang JY, Chen YP, Xia TH, Wang LZ et al. Bessel terahertz pulses from superluminal laser plasma filaments. *Ultrafast Sci* **2022**, 9870325 (2022).
43. Mitrofanov AV, Sidorov-Biryukov DA, Nazarov MM, Voronin AA, Rozhko MV et al. Ultraviolet-to-millimeter-band supercontinua driven by ultrashort mid-infrared laser pulses. *Optica* **7**, 15–19 (2020).
44. Fülöp JA, Tzortzakis S, Kampfrath T. Laser-driven strong-field terahertz sources. *Adv Opt Mater* **8**, 1900681 (2020).
45. Löffler T, Kress M, Thomson M, Roskos HG. Efficient terahertz pulse generation in laser-induced gas plasmas. *Acta Phys Pol A* **107**, 99–108 (2005).
46. Hamster H. Generation of sub-picosecond terahertz radiation by laser-produced plasmas. (University of California, Berkeley, 1993).
47. Hora H. *Laser Plasma Physics*: *Forces and the Nonlinearity Principle* (SPIE, Bellingham, 2000).
48. Sprangle P, Peñano JR, Hafizi B, Kapetanakos CA. Ultrashort laser pulses and electromagnetic pulse generation in air and on dielectric surfaces. *Phys Rev E* **69**, 066415 (2004).
49. Cheng CC, Wright EM, Moloney JV. Generation of electromagnetic pulses from plasma channels induced by femtosecond light strings. *Phys Rev Lett* **87**, 213001 (2001).
50. Shkurinov AP, Sinko AS, Solyankin PM, Borodin AV, Esaulkov MN et al. Impact of the dipole contribution on the terahertz emission of air-based plasma induced by tightly focused femtosecond laser pulses. *Phys Rev E* **95**, 043209 (2017).
51. Kolesik M, Moloney JV, Mlejnek M. Unidirectional optical pulse propagation equation. *Phys Rev Lett* **89**, 283902 (2002).
52. Kolesik M, Moloney JV. Nonlinear optical pulse propagation simulation: from Maxwell's to unidirectional equations. *Phys Rev E* **70**, 036604 (2004).
53. Babushkin I, Kuehn W, Köhler C, Skupin S, Bergé L et al. Ultrafast spatiotemporal dynamics of terahertz generation by ionizing two-color femtosecond pulses in gases. *Phys Rev Lett* **105**, 053903 (2010).
54. Babushkin I, Skupin S, Husakou A, Köhler C, Cabrera-Granado E et al. Tailoring terahertz radiation by controlling tunnel photoionization events in gases. *New J Phys* **13**, 123029 (2011).
55. Bergé L, Skupin S, Köhler C, Babushkin I, Herrmann J. 3D numerical simulations of THz generation by two-color laser filaments. *Phys Rev Lett* **110**, 073901 (2013).
56. Nguyen A, Kaltenecker KJ, Delagnes JC, Zhou B, Cormier E et al. Wavelength scaling of terahertz pulse energies delivered by two-color air plasmas. *Opt Lett* **44**, 1488–1491 (2019).
57. D'Amico C, Houard A, Franco M, Prade B, Mysyrowicz A et al. Conical forward THz emission from femtosecond-laser-beam filamentation in air. *Phys Rev Lett* **98**, 235002 (2007).
58. Amico CD, Houard A, Akturk S, Liu Y, Le Bloas J et al. Forward THz radiation emission by femtosecond filamentation in gases: theory and experiment. *New J Phys* **10**, 013015 (2008).
59. Cook DJ, Hochstrasser RM. Intense terahertz pulses by four-wave rectification in air. *Opt Lett* **25**, 1210–1212 (2000).
60. Kress M, Löffler T, Eden S, Thomson M, Roskos HG. Terahertz-pulse generation by photoionization of air with laser pulses composed of both fundamental and second-harmonic waves. *Opt Lett* **29**, 1120–1122 (2004).
61. Xie X, Dai JM, Zhang XC. Coherent control of THz wave generation in ambient air. *Phys Rev Lett* **96**, 075005 (2006).
62. Houard A, Liu Y, Prade B, Mysyrowicz A. Polarization analysis of terahertz radiation generated by four-wave mixing in air. *Opt Lett* **33**, 1195–1197 (2008).
63. Kim KY, Glownia JH, Taylor AJ, Rodriguez G. Terahertz emission from ultrafast ionizing air in symmetry-broken laser fields. *Opt Express* **15**, 4577–4584 (2007).
64. Kim KY, Taylor AJ, Glownia JH, Rodriguez G. Coherent control of terahertz supercontinuum generation in ultrafast laser–gas interactions. *Nat Photonics* **2**, 605–609 (2008).
65. de Alaiza Martínez PG, Babushkin I, Bergé L, Skupin S, Cabrera-Granado E et al. Boosting terahertz generation in laser-field ionized gases using a sawtooth wave shape. *Phys Rev Lett* **114**, 183901 (2015).
66. Lu CH, Zhang CY, Zhang LQ, Wang XW, Zhang SA. Modulation of terahertz-spectrum generation from an air plasma by tunable three-color laser pulses. *Phys Rev A* **96**, 053402 (2017).
67. Liu SJ, Fan ZQ, Lu CH, Gui JY, Luo C et al. Coherent control of boosted terahertz radiation from air plasma pumped by a femtosecond three-color sawtooth field. *Phys Rev A* **102**, 063522 (2020).
68. Andreeva VA, Kosareva OG, Panov NA, Shipilo DE, Solyankin PM et al. Ultrabroad terahertz spectrum generation from an air-based filament plasma. *Phys Rev Lett* **116**, 063902 (2016).
69. Vaičaitis V, Ivanov M, Adomavičius K, Svirskas Ž, Morgner U et al. Influence of laser-preformed plasma on THz wave generation in air by bichromatic laser pulses. *Laser Phys* **28**, 095402

(2018).
70. Houard A, Liu Y, Prade B, Tikhonchuk VT, Mysyrowicz A. Strong enhancement of terahertz radiation from laser filaments in air by a static electric field. *Phys Rev Lett* **100**, 255006 (2008).
71. Sun WF, Zhou YS, Wang XK, Zhang Y. External electric field control of THz pulse generation in ambient air. *Opt Express* **16**, 16573–16580 (2008).
72. Wang TJ, Ju JJ, Liu YX, Li RX, Xu ZX et al. Waveform control of enhanced THz radiation from femtosecond laser filament in air. *Appl Phys Lett* **110**, 221102 (2017).
73. Liu Y, Houard A, Prade B, Mysyrowicz A, Diaw A et al. Amplification of transition-Cherenkov terahertz radiation of femtosecond filament in air. *Appl Phys Lett* **93**, 051108 (2008).
74. D'Amico C, Houard A, Franco M, Prade B, Mysyrowicz A. Coherent and incoherent radial THz radiation emission from femtosecond filaments in air. *Opt Express* **15**, 15274–15279 (2007).
75. Zhao JY, Guo LJ, Chu W, Zeng B, Gao H et al. Simple method to enhance terahertz radiation from femtosecond laser filament array with a step phase plate. *Opt Lett* **40**, 3838–3841 (2015).
76. Song QY, Yuan XM, Hu SS, Huang JF, Zhong HZ et al. Enhance terahertz radiation and its polarization- control with two paralleled filaments pumped by two-color femtosecond laser fields. *Opt Express* **29**, 22659–22666 (2021).
77. Liu Y, Houard A, Prade B, Akturk S, Mysyrowicz A et al. Terahertz radiation source in air based on bifilamentation of femtosecond laser pulses. *Phys Rev Lett* **99**, 135002 (2007).
78. Panov N, Andreeva V, Kosareva O, Shkurinov A, Makarov VA et al. Directionality of terahertz radiation emitted from an array of femtosecond filaments in gases. *Laser Phys Lett* **11**, 125401 (2014).
79. Mitryukovskiy SI, Liu Y, Prade B, Houard A, Mysyrowicz A. Coherent synthesis of terahertz radiation from femtosecond laser filaments in air. *Appl Phys Lett* **102**, 221107 (2013).
80. Manceau JM, Averchi A, Bonaretti F, Faccio D, Di Trapani P et al. Terahertz pulse emission optimization from tailored femtosecond laser pulse filamentation in air. *Opt Lett* **34**, 2165–2167 (2009).
81. Wang WM, Sheng ZM, Dong XG, Du HW, Li YT et al. Controllable far-infrared electromagnetic radiation from plasmas applied by dc or ac bias electric fields. *J Appl Phys* **107**, 023113 (2010).
82. Yoo YJ, Kuk D, Zhong ZQ, Kim KY. Generation and characterization of strong terahertz fields from kHz laser filamentation. *IEEE J Sel Top Quantum Electron* **23**, 8501007 (2016).
83. Alirezaee H, Sharifian M. Contribution of photocurrent mechanism and influence of plasma length in THz generation by two-color laser induced plasma. *Phys Plasmas* **25**, 043112 (2018).
84. Chen M, Yuan XH, Sheng ZM. Scalable control of terahertz radiation from ultrashort laser-gas interaction. *Appl Phys Lett* **101**, 161908 (2012).
85. Liu K, Koulouklidis AD, Papazoglou DG, Tzortzakis S, Zhang XC. Enhanced terahertz wave emission from air-plasma tailored by abruptly autofocusing laser beams. *Optica* **3**, 605–608 (2016).
86. Hah J, Jiang W, He ZH, Nees JA, Hou B et al. Enhancement of THz generation by feedback-optimized wavefront manipulation. *Opt Express* **25**, 17271–17279 (2017).
87. Kuk D, Yoo YJ, Rosenthal EW, Jhajj N, Milchberg HM et al. Generation of scalable terahertz radiation from cylindrically focused two-color laser pulses in air. *Appl Phys Lett* **108**, 121106 (2016).
88. Su Q, Liu WW, Lu D, Qi PF, Kosareva O et al. Influence of the tilting angle of a BBO crystal on the terahertz radiation produced by a dual-color femtosecond laser. *IEEE Trans Terahertz Sci Technol* **9**, 669–674 (2019).
89. Li H, Zhang Y, Sun WF, Wang XK, Feng SF et al. Contribution of the optical rectification in terahertz radiation driven by two-color laser induced plasma. *Opt Express* **28**, 4810–4816 (2020).
90. Xie J, Fan WH, Chen X. Systematic experimental study on a highly efficient terahertz source based on two-color laser-induced air plasma. *Laser Phys* **26**, 055002 (2016).
91. Buccheri F, Zhang XC. Terahertz emission from laser-induced microplasma in ambient air. *Optica* **2**, 366–369 (2015).
92. Jang D, Schwartz RM, Woodbury D, Griff-McMahon J, Younis AH et al. Efficient terahertz and Brunel harmonic generation from air plasma via mid-infrared coherent control. *Optica* **6**, 1338–1341 (2019).
93. Fedorov VY, Tzortzakis S. Optimal wavelength for two-color filamentation-induced terahertz sources. *Opt Express* **26**, 31150–31159 (2018).
94. Nguyen A, de Alaiza Martínez PG, Thiele I, Skupin S, Bergé L. Broadband terahertz radiation from two-color mid- and far-infrared laser filaments in air. *Phys Rev A* **97**, 063839 (2018).
95. Wang WM, Kawata S, Sheng ZM, Li YT, Chen LM et al. Efficient terahertz emission by mid-infrared laser pulses from gas targets. *Opt Lett* **36**, 2608–2610 (2011).
96. Koulouklidis AD, Gollner C, Shumakova V, Fedorov VY, Pugžlys A et al. Observation of extremely efficient terahertz generation from mid-infrared two-color laser filaments. *Nat Commun* **11**, 292 (2020).
97. Meng C, Chen WB, Wang XW, Lü ZH, Huang YD et al. Enhancement of terahertz radiation by using circularly polarized two-color laser fields. *Appl Phys Lett* **109**, 131105 (2016).
98. Tailliez C, Stathopulos A, Skupin S, Buožius D, Babushkin I et al. Terahertz pulse generation by two-color laser fields with circular polarization. *New J Phys* **22**, 103038 (2020).
99. Wang SX, Lu CH, Fan ZQ, Houard A, Tikhonchuk V et al. Coherently controlled ionization of gases by three-color femtosecond laser pulses. *Phys Rev A* **105**, 023529 (2022).
100. Vaičaitis V, Balachninaitė O, Morgner U, Babushkin I. Terahertz radiation generation by three-color laser pulses in air filament. *J Appl Phys* **125**, 173103 (2019).
101. Vvedenskii NV, Korytin AI, Kostin VA, Murzanev AA, Silaev AA et al. Two-color laser-plasma generation of terahertz radiation using a frequency-tunable half harmonic of a femtosecond pulse. *Phys Rev Lett* **112**, 055004 (2014).
102. Wang WM, Li YT, Sheng ZM, Lu X, Zhang J. Terahertz radiation by two-color lasers due to the field ionization of gases. *Phys Rev E* **87**, 033108 (2013).
103. Zhang LL, Wang WM, Wu T, Zhang R, Zhang SJ et al. Observation of terahertz radiation via the two-color laser scheme with uncommon frequency ratios. *Phys Rev Lett* **119**, 235001 (2017).
104. Zhang Z, Panov N, Andreeva V, Zhang ZL, Slepkov A et al. Optimum chirp for efficient terahertz generation from two-color femtosecond pulses in air. *Appl Phys Lett* **113**, 241103 (2018).

105. Wang WM, Sheng ZM, Wu HC, Chen M, Li C et al. Strong terahertz pulse generation by chirped laser pulses in tenuous gases. *Opt Express* **16**, 16999–17006 (2008).
106. Wang WM, Kawata S, Sheng ZM, Li YT, Zhang J. Towards gigawatt terahertz emission by few-cycle laser pulses. *Phys Plasmas* **18**, 073108 (2011).
107. Nguyen A, de Alaiza Martínez PG, Thiele I, Skupin S, Bergé L. THz field engineering in two-color femtosecond filaments using chirped and delayed laser pulses. *New J Phys* **20**, 033026 (2018).
108. Dai JM, Xie X, Zhang XC. Detection of broadband terahertz waves with a laser-induced plasma in gases. *Phys Rev Lett* **97**, 103903 (2006).
109. Clough B, Liu JL, Zhang XC. "All air–plasma" terahertz spectroscopy. *Opt Lett* **36**, 2399–2401 (2011).
110. Blank V, Thomson MD, Roskos HG. Spatio-spectral characteristics of ultra-broadband THz emission from two-colour photo-excited gas plasmas and their impact for nonlinear spectroscopy. *New J Phys* **15**, 075023 (2013).
111. Chen YP, Zhang ZL, Zhang Z, Yuan XH, Liu F et al. Spectral interference of terahertz pulses from two laser filaments in air. *Appl Phys Lett* **106**, 221105 (2015).
112. Zhang ZL, Chen YP, Yang L, Yuan XH, Liu F et al. Dual-frequency terahertz emission from splitting filaments induced by lens tilting in air. *Appl Phys Lett* **105**, 101110 (2014).
113. He BQ, Nan JY, Li M, Yuan S, Zeng HP. Terahertz modulation induced by filament interaction. *Opt Lett* **42**, 967–970 (2017).
114. Du HW, Hoshina H, Otani C, Midorikawa K. Terahertz waves radiated from two noncollinear femtosecond plasma filaments. *Appl Phys Lett* **107**, 211113 (2015).
115. Zhang Y, Sun WF, Wang XK, Ye JS, Feng SF et al. Active modulation of the terahertz spectra radiated from two air plasmas. *Opt Lett* **42**, 1907–1910 (2017).
116. Li M, Yuan S, Zeng HP. THz frequency modulation by filamentary plasma grating. *IEEE J Sel Top Quantum Electron* **23**, 8400604 (2017).
117. Sheng W, Tang F, Zhang ZL, Chen YP, Peng XY et al. Spectral control of terahertz radiation from inhomogeneous plasma filaments by tailoring two-color laser beams. *Opt Express* **29**, 8676–8684 (2021).
118. Minami Y, Kurihara T, Yamaguchi K, Nakajima M, Suemoto T. Longitudinal terahertz wave generation from an air plasma filament induced by a femtosecond laser. *Appl Phys Lett* **102**, 151106 (2013).
119. Dai JM, Karpowicz N, Zhang XC. Coherent polarization control of terahertz waves generated from two-color laser-induced gas plasma. *Phys Rev Lett* **103**, 023001 (2009).
120. You YS, Oh TI, Kim KY. Mechanism of elliptically polarized terahertz generation in two-color laser filamentation. *Opt Lett* **38**, 1034–1036 (2013).
121. Chen YP, Marceau C, Génier S, Théberge F, Châteauneuf M et al. Elliptically polarized terahertz emission through four-wave mixing in a two-color filament in air. *Opt Commun* **282**, 4283–4287 (2009).
122. Zhang Y, Chen Y, Marceau C, Liu W, Sun ZD et al. Non-radially polarized THz pulse emitted from femtosecond laser filament in air. *Opt Express* **16**, 15483–15488 (2008).
123. Smirnov SV, Kulya MS, Tcypkin AN, Putilin SE, Bespalov VG. Detection of the polarization spatial distribution of THz radiation generated by two-color laser filamentation. *Nanosyst Phys Chem Math* **8**, 613–619 (2017).
124. Xie D, Zhang H, Yin Y, Wang J, Yu TP. Tunable elliptically polarized Hermite-Gaussian terahertz radiation driven by two-color twisted laser pulses. *Opt Express* **28**, 33784–33794 (2020).
125. Fedorov VY, Koulouklidis AD, Tzortzakis S. THz generation by two-color femtosecond filaments with complex polarization states: four-wave mixing versus photocurrent contributions. *Plasma Phys Control Fusion* **59**, 014025 (2017).
126. Lu XF, Zhang XC. Generation of elliptically polarized terahertz waves from laser-induced plasma with double helix electrodes. *Phys Rev Lett* **108**, 123903 (2012).
127. Su Q, Xu Q, Zhang N, Zhang Y, Liu WW. Control of terahertz pulse polarization by two crossing DC fields during femtosecond laser filamentation in air. *J Opt Soc Am B* **36**, G1–G5 (2019).
128. Kosareva O, Esaulkov M, Panov N, Andreeva V, Shipilo D et al. Polarization control of terahertz radiation from two-color femtosecond gas breakdown plasma. *Opt Lett* **43**, 90–93 (2018).
129. Jahangiri F, Hashida M, Tokita S, Nagashima T, Hangyo M et al. Directional elliptically polarized terahertz emission from air plasma produced by circularly polarized intense femtosecond laser pulses. *Appl Phys Lett* **99**, 161505 (2011).
130. Zhong H, Karpowicz N, Zhang XC. Terahertz emission profile from laser-induced air plasma. *Appl Phys Lett* **88**, 261103 (2006).
131. Akhmedzhanov RA, Ilyakov IE, Mironov VA, Suvorov EV, Fadeev DA et al. Generation of terahertz radiation by the optical breakdown induced by a bichromatic laser pulse. *J Exp Theor Phys* **109**, 370–378 (2009).
132. You YS, Oh TI, Kim KY. Off-axis phase-matched terahertz emission from two-color laser-induced plasma filaments. *Phys Rev Lett* **109**, 183902 (2012).
133. Gorodetsky A, Koulouklidis AD, Massaouti M, Tzortzakis S. Physics of the conical broadband terahertz emission from two-color laser-induced plasma filaments. *Phys Rev A* **89**, 033838 (2014).
134. Klarskov P, Strikwerda AC, Iwaszczuk K, Jepsen PU. Experimental three-dimensional beam profiling and modeling of a terahertz beam generated from a two-color air plasma. *New J Phys* **15**, 075012 (2013).
135. Chizhov PA, Ushakov AA, Bukin VV, Garnov SV. Measurement of spatio-temporal field distribution of THz pulses in electro-optic crystal by interferometry method. *Quantum Electron* **45**, 434–436 (2015).
136. Wang XK, Cui Y, Sun WF, Ye JS, Zhang Y. Terahertz real-time imaging with balanced electro-optic detection. *Opt Commun* **283**, 4626–4632 (2010).
137. Wang EL, Wang YL, Sun WF, Wang XK, Feng SF et al. Spatiotemporal distribution characterization for terahertz waves generated from plasma induced by two-color pulses. *Front Phys* **9**, 768186 (2021).
138. Koribut AV, Rizaev GE, Mokrousova DV, Savinov SA, Reutov AA et al. Similarity of angular distribution for THz radiation emitted by laser filament plasma channels of different lengths. *Opt Lett* **45**, 4009–4011 (2020).
139. Sørensen CB, Guiramand L, Degert J, Tondusson M, Skovsen E et al. Conical versus Gaussian terahertz emission from two-color laser-induced air plasma filaments. *Opt Lett* **45**, 2132–2135 (2020).

140. Ushakov AA, Chizhov PA, Andreeva VA, Panov NA, Shipilo DE et al. Ring and unimodal angular-frequency distribution of THz emission from two-color femtosecond plasma spark. *Opt Express* **26**, 18202–18213 (2018).
141. Thrane L, Jacobsen RH, Jepsen PU, Keiding SR. THz reflection spectroscopy of liquid water. *Chem Phys Lett* **240**, 330–333 (1995).
142. E YW, Zhang LL, Tsypkin A, Kozlov S, Zhang CL et al. Progress, challenges, and opportunities of terahertz emission from liquids. *J Opt Soc Am B* **39**, A43–A51 (2022).
143. Jin Q, E YW, Williams K, Dai JM, Zhang XC. Observation of broadband terahertz wave generation from liquid water. *Appl Phys Lett* **111**, 071103 (2017).
144. E YW, Jin Q, Tcypkin A, Zhang XC. Terahertz wave generation from liquid water films via laser-induced breakdown. *Appl Phys Lett* **113**, 181103 (2018).
145. Feng SJ, Dong LQ, Wu T, Tan Y, Zhang R et al. Terahertz wave emission from water lines. *Chin Opt Lett* **18**, 023202 (2020).
146. Zhang LL, Wang WM, Wu T, Feng SJ, Kang K et al. Strong terahertz radiation from a liquid-water line. *Phys Rev Appl* **12**, 014005 (2019).
147. Tcypkin AN, Ponomareva EA, Putilin SE, Smirnov SV, Shtumpf SA et al. Flat liquid jet as a highly efficient source of terahertz radiation. *Opt Express* **27**, 15485–15494 (2019).
148. Stumpf S, Ponomareva E, Tcypkin A, Putilin S, Korolev A et al. Temporal field and frequency spectrum of intense femtosecond radiation dynamics in the process of plasma formation in a dielectric medium. *Laser Phys* **29**, 124014 (2019).
149. Dey I, Jana K, Fedorov VY, Koulouklidis AD, Mondal A et al. Highly efficient broadband terahertz generation from ultrashort laser filamentation in liquids. *Nat Commun* **8**, 1184 (2017).
150. Wang HY, Shen T. Unified theoretical model for both one- and two-color laser excitation of terahertz waves from a liquid. *Appl Phys Lett* **117**, 131101 (2020).
151. Lu CH, He T, Zhang LQ, Zhang H, Yao YH et al. Effect of two-color laser pulse duration on intense terahertz generation at different laser intensities. *Phys Rev A* **92**, 063850 (2015).
152. Chen YX, He YH, Zhang YF, Tian Z, Dai JM. Systematic investigation of terahertz wave generation from liquid water lines. *Opt Express* **29**, 20477–20486 (2021).
153. Jin Q, E YW, Gao SH, Zhang XC. Preference of subpicosecond laser pulses for terahertz wave generation from liquids. *Adv Photonics* **2**, 015001 (2020).
154. Li M, Li ZY, Nan JY, Xia Y, He MY et al. THz generation from water wedge excited by dual-color pulse. *Chin Opt Lett* **18**, 073201 (2020).
155. Jin Q, E YW, Zhang XC. Terahertz aqueous photonics. *Front Optoelectron* **14**, 37–63 (2021).
156. Jin Q, Dai JM, E YW, Zhang XC. Terahertz wave emission from a liquid water film under the excitation of asymmetric optical fields. *Appl Phys Lett* **113**, 261101 (2018).
157. Danson C, Hillier D, Hopps N, Neely D. Petawatt class lasers worldwide. *High Power Laser Sci Eng* **3**, e3 (2015).
158. Mourou GA, Tajima T, Bulanov SV. Optics in the relativistic regime. *Rev Mod Phys* **78**, 309–371 (2006).
159. Hamster H, Sullivan A, Gordon S, White W, Falcone RW. Subpicosecond, electromagnetic pulses from intense laser-plasma interaction. *Phys Rev Lett* **71**, 2725–2728 (1993).
160. Hamster H, Sullivan A, Gordon S, Falcone RW. Short-pulse terahertz radiation from high-intensity-laser-produced plasmas. *Phys Rev E* **49**, 671–677 (1994).
161. Gopal A, Singh P, Herzer S, Reinhard A, Schmidt A et al. Characterization of 700 μJ T rays generated during high-power laser solid interaction. *Opt Lett* **38**, 4705–4707 (2013).
162. Hinkel-Lipsker DE, Fried BD, Morales GJ. Analytic expression for mode conversion of Langmuir and electromagnetic waves. *Phys Rev Lett* **62**, 2680–2682 (1989).
163. Liao GQ, Li YT. Review of intense terahertz radiation from relativistic laser-produced plasmas. *IEEE Trans Plasma Sci* **47**, 3002–3008 (2019).
164. Yoshii J, Lai CH, Katsouleas T, Joshi C, Mori WB. Radiation from Cerenkov wakes in a magnetized plasma. *Phys Rev Lett* **79**, 4194–4197 (1997).
165. Liao GQ, Li YT, Li C, Su LN, Zheng Y et al. Bursts of terahertz radiation from large-scale plasmas irradiated by relativistic picosecond laser pulses. *Phys Rev Lett* **114**, 255001 (2015).
166. Wu HC, Sheng ZM, Zhang J. Single-cycle powerful megawatt to gigawatt terahertz pulse radiated from a wavelength-scale plasma oscillator. *Phys Rev E* **77**, 046405 (2008).
167. Chen ZY, Li XY, Yu W. Intense terahertz emission from relativistic circularly polarized laser pulses interaction with overdense plasmas. *Phys Plasmas* **20**, 103115 (2013).
168. Sagisaka A, Daido H, Nashima S, Orimo S, Ogura K et al. Simultaneous generation of a proton beam and terahertz radiation in high-intensity laser and thin-foil interaction. *Appl Phys B* **90**, 373–377 (2008).
169. Li YT, Li C, Zhou ML, Wang WM, Du F et al. Strong terahertz radiation from relativistic laser interaction with solid density plasmas. *Appl Phys Lett* **100**, 254101 (2012).
170. Nakamura T, Kato S, Nagatomo H, Mima K. Surface-magnetic-field and fast-electron current-layer formation by ultraintense laser irradiation. *Phys Rev Lett* **93**, 265002 (2004).
171. Li YT, Yuan XH, Xu MH, Zheng ZY, Sheng ZM et al. Observation of a fast electron beam emitted along the surface of a target irradiated by intense femtosecond laser pulses. *Phys Rev Lett* **96**, 165003 (2006).
172. Liao GQ, Li YT, Li C, Mondal S, Hafez HA et al. Terahertz emission from two-plasmon-decay induced transient currents in laser-solid interactions. *Phys Plasmas* **23**, 013104 (2016).
173. Li C, Liao GQ, Zhou ML, Du F, Ma JL et al. Backward terahertz radiation from intense laser-solid interactions. *Opt Express* **24**, 4010–4021 (2016).
174. Ginzburg VL, Frank IM. Radiation of a uniformly moving electron due to its transition from one medium into another. *J Phys* **9**, 353–362 (1945).
175. Herzer S, Woldegeorgis A, Polz J, Reinhard A, Almassarani M et al. An investigation on THz yield from laser-produced solid density plasmas at relativistic laser intensities. *New J Phys* **20**, 063019 (2018).
176. Gopal A, Herzer S, Schmidt A, Singh P, Reinhard A et al. Observation of gigawatt-class THz pulses from a compact laser-driven particle accelerator. *Phys Rev Lett* **111**, 074802 (2013).
177. Mora P. Plasma expansion into a vacuum. *Phys Rev Lett* **90**, 185002 (2003).
178. Déchard J, Davoine X, Gremillet L, Bergé L. Terahertz emission from submicron solid targets irradiated by ultraintense femtosecond laser pulses. *Phys Plasmas* **27**, 093105 (2020).
179. Leemans WP, Geddes CGR, Faure J, Tóth C, van Tilborg J et al. Observation of terahertz emission from a laser-plasma

accelerated electron bunch crossing a plasma-vacuum boundary. *Phys Rev Lett* **91**, 074802 (2003).
180. Schroeder CB, Esarey E, van Tilborg J, Leemans WP. Theory of coherent transition radiation generated at a plasma-vacuum interface. *Phys Rev E* **69**, 016501 (2004).
181. Yang X, Brunetti E, Jaroszynski DA. High-energy coherent terahertz radiation emitted by wide-angle electron beams from a laser-wakefield accelerator. *New J Phys* **20**, 043046 (2018).
182. Liao GQ, Li YT, Zhang YH, Liu H, Ge XL et al. Demonstration of coherent terahertz transition radiation from relativistic laser-solid interactions. *Phys Rev Lett* **116**, 205003 (2016).
183. Liao GQ, Li YT, Liu H, Scott GG, Neely D et al. Multimillijoule coherent terahertz bursts from picosecond laser-irradiated metal foils. *Proc Natl Acad Sci USA* **116**, 3994–3999 (2019).
184. Fedeli L, Formenti A, Cialfi L, Sgattoni A, Cantono G et al. Structured targets for advanced laser-driven sources. *Plasma Phys Control Fusion* **60**, 014013 (2018).
185. Mondal S, Wei Q, Ding WJ, Hafez HA, Fareed MA et al. Aligned copper nanorod arrays for highly efficient generation of intense ultra-broadband THz pulses. *Sci Rep* **7**, 40058 (2017).
186. Li C, Zhou ML, Ding WJ, Du F, Liu F et al. Effects of laser-plasma interactions on terahertz radiation from solid targets irradiated by ultrashort intense laser pulses. *Phys Rev E* **84**, 036405 (2011).
187. Li C, Cui YQ, Zhou ML, Du F, Li YT et al. Role of resonance absorption in terahertz radiation generation from solid targets. *Opt Express* **22**, 11797–11803 (2014).
188. Jin Z, Zhuo HB, Nakazawa T, Shin JH, Wakamatsu S et al. Highly efficient terahertz radiation from a thin foil irradiated by a high-contrast laser pulse. *Phys Rev E* **94**, 033206 (2016).
189. Woldegeorgis A, Kurihara T, Almassarani M, Beleites B, Grosse R et al. Multi-MV/cm longitudinally polarized terahertz pulses from laser–thin foil interaction. *Optica* **5**, 1474–1477 (2018).
190. Déchard J, Debayle A, Davoine X, Gremillet L, Bergé L. Terahertz pulse generation in underdense relativistic plasmas: From photoionization-induced radiation to coherent transition radiation. *Phys Rev Lett* **120**, 144801 (2018).
191. Déchard J, Davoine X, Bergé L. THz generation from relativistic plasmas driven by near-to far-infrared laser pulses. *Phys Rev Lett* **123**, 264801 (2019).

Acknowledgements

This work was supported by the National Natural Science Foundation of China (Grant Nos. 11774246 and 121774271), the National Key R&D Program of China (Grant No. 2019YFC1711905), the Beijing Talents Project (Grant No. 2018A19), the Sino-German Mobility Program of the Sino-German Center for Science Funding (Grant No. M-0225), the Capacity Building for Science & Technology Innovation-Fundamental Scientific Research Funds (Grant No. 00820531120017).

Competing interests

The authors declare no competing financial interests.